Crystallographic Topology and Its Applications*

Carroll K. Johnson and Michael N. Burnett
Chemical and Analytical Sciences Division, Oak Ridge National Laboratory
Oak Ridge, TN 37831-6197, USA
ckj@ornl.gov
http://www.ornl.gov/ortep/topology.html

William D. Dunbar
Division of Natural Sciences & Mathematics, Simon's Rock College
Great Barrington, MA 01230, USA
wdunbar@plato.simons-rock.edu
http://www.simons-rock.edu/~wdunbar

Abstract

Geometric topology and structural crystallography concepts are combined to define a new area we call Structural Crystallographic Topology, which may be of interest to both crystallographers and mathematicians.

In this paper, we represent crystallographic symmetry groups by orbifolds and crystal structures by Morse functions. The Morse function uses mildly overlapping Gaussian thermal-motion probability density functions centered on atomic sites to form a critical net with peak, pass, pale, and pit critical points joined into a graph by density gradient-flow separatrices. Critical net crystal structure drawings can be made with the ORTEP-III graphics program.

An orbifold consists of an underlying topological space with an embedded singular set that represents the Wyckoff sites of the crystallographic group. An orbifold for a point group, plane group, or space group is derived by gluing together equivalent edges or faces of a crystallographic asymmetric unit.

The critical-net-on-orbifold model incorporates the classical invariant lattice complexes of crystallography and allows concise quotient-space topological illustrations to be drawn without the repetition that is characteristic of normal crystal structure drawings.

1. Introduction

For our purpose we will say that crystallography is the study of atoms in crystals, topology is the study of distortion-invariant properties of mathematical objects, and crystallographic topology is an intersection of those two disciplines. Since both topology and crystallography have many subdisciplines, there are a number of quite different intersection regions that can be called crystallographic topology; but we will confine this discussion to one well delineated subarea.

The structural crystallography of interest involves the group theory required to describe symmetric arrangements of atoms in crystals and a classification of the simplest arrangements as lattice complexes. The geometric topology of interest is the topological properties of crystallographic groups, represented as orbifolds, and the Morse theory global analysis of critical points in symmetric functions. Here we are taking the liberty of calling global analysis part of topology.

Our basic approach is that of geometric crystallographers who find the pictorial reasoning of geometric topology intriguing. From a mathematical perspective, one can reformulate the subject using algebraic topology concepts such as cohomology, which we seldom mention in this paper.

The International Tables for Crystallography (ITCr), Volume A: Space-Group Symmetry[1] is the chief source for the crystallographic material in the following discussion. It is our hope that the discipline of "Crystallographic Topology" will mature in completeness and usefulness to justify the addition of this subject to the ITCr series at some future time.

There are a number of crystallographic and topological concepts that lead to the following mappings of structural crystallography onto geometric topology. Only the first two of the three mapping series are discussed here.

Crystallographic Groups → Spherical and Euclidean Orbifolds

* Research sponsored by the Laboratory Directed Research and Development Program of the Oak Ridge National Laboratory, managed by Lockheed Martin Energy Research Corp. for the U.S. Department of Energy under Contract No. DE-AC05-96OR22464.

Crystal Structures → Morse Functions → Critical Nets → Critical Nets on Orbifolds → Lattice Complexes on Critical Nets on Orbifolds

Crystal Chemistry → Convolution of Chemical Motif Critical Nets onto Orbifold Singular Sets

1.1 Organization

Sect. 1 provides an overview and illustrates a simple critical net, orbifold, and critical net on orbifold based on the sodium chloride crystal structure. Following a review of relevant orbifold references, Sect. 2 continues to illustrate and classify the 32 spherical 2-orbifolds derived from the crystallographic point groups and shows how spherical 2-orbifolds can be used as construction elements to build the singular sets of Euclidean 3-orbifolds. Sect. 2 also illustrates basic topology surfaces, derivation of all 17 Euclidean 2-orbifolds from crystallographic drawings of the plane groups, and example derivations of Euclidean 3-orbifolds by lifting base Euclidean 2-orbifolds. Some of the singular sets of the polar space group orbifolds are illustrated since polar space groups are the ones of chief interest to biological crystallographers.

Sect. 3 describes the Morse functions used and shows additional critical net examples, using ORTEP illustrations, and summarizes their characteristics. Sect. 4 illustrates the derivation of critical nets on orbifolds, their presentation in linearized form, and the derivation of a symmetry-breaking family of cubic lattice complexes on orbifolds. The crystallographic lattice complex model as modified for critical nets on orbifolds is discussed in Sect. 5. Sect. 6 summarizes the current status of crystallographic topology and the future developments required to make it a productive subfield of contemporary crystallography. The Appendix shows a group/subgroup graph for the cubic space groups.

A Crystallographic Orbifold Atlas (in preparation) will eventually provide a full tabulation of those topological properties of crystallographic orbifolds that seem potentially useful to crystallographers. We have basic results covering most of the space groups, but at present we have not developed an optimal format or adequate graphics automation for their presentation.

1.2 Critical Nets

Critical nets are based on the concepts of Morse functions and Morse theory[2,3,4,5] (i.e., critical point analysis), which are classic topics in the mathematical topology and global analysis literature.

Our recently released ORTEP-III computer program[6] can produce "critical net" illustrations that depict some canonical topological characteristics of the ensemble of overlapping atomic-thermal-motion Gaussian density functions in a crystal. Only non-degenerate critical points are considered here since a degenerate critical point can always be distorted into a set of non-degenerate ones through small perturbations.[7,8] We have so far not found a true degenerate critical point in a valid crystal structure and have a working hypothesis that all crystal structures are Morse functions, which are named after Marston Morse[2] and have no degenerate critical points.

Critical points occur where the first derivative of the global density is zero. The second derivative at that point is a 3×3 symmetric matrix, which has a non-zero determinant only if the critical point is non-degenerate. The signs of the three eigenvalues of the second derivative matrix specify the types of critical points, which we term peak (-,-,-), pass (+,-,-), pale (+,+,-) and pit (+,+,+). A degenerate critical point will have a singular second derivative matrix with one or more zero or nearly zero eigenvalues.

The critical points are best described as representing 0-, 1-, 2-, and 3-dimensional cells in a topological Morse function CW complex (i.e., C for closure finite, W for weak topology). We use a "critical net" representation that has unique topological "separatrices" joining the critical point nodes into a graph. We denote the peak, pass, pale, and pit critical points with the numbers 0, 1, 2, and 3, respectively. The most gradual down-density paths from a peak to a pit follow the sequence peak → pass → pale → pit. These paths, shown by the separatrices (i.e., "connection links") in Figs. 1.1 and 1.2, are topologically unique. This uniqueness arises because: (a) the pass and pale critical points each have one unique eigenvector connecting to the separatrices going to one peak and one pit, respectively, and (b) there are two-dimensional hyperplanes connecting to the two remaining eigenvectors of each pass and pale and these non-parallel hyperplanes intersect each other locally to form the pass-pale separatrices.

We postulate that there are no bifurcated (forked) separatrices or degenerate critical points in the crystallographic critical nets of interest here. In experimentally derived crystallographic macromolecule electron-density functions, this will not be the case because of critical point merging caused by inadequate resolution experimental data and lattice-averaged static disorder. Theoretical quantum chemistry and high precision x-ray structure results may also lead to exceptions because of added quantum chemistry topological features.[9]

1.3 Critical Net for NaCl

Fig. 1.1 is an ORTEP-III critical net illustration for one octant of the NaCl unit cell contents with the larger corner spheres representing Cl peaks; the smaller corner spheres, Na peaks; the cigar-shaped ellipsoids, passes; the pancake-shaped ellipsoids, pales; and the smallest sphere in the center, a pit. The reason for this choice of shapes for the pass and pale saddle points is that in the simplest examples the passes and pales represent edges and faces, respectively, for convex polyhedra in special cases such as NaCl. Non-polyhedral counterexamples are discussed in Sect. 3.

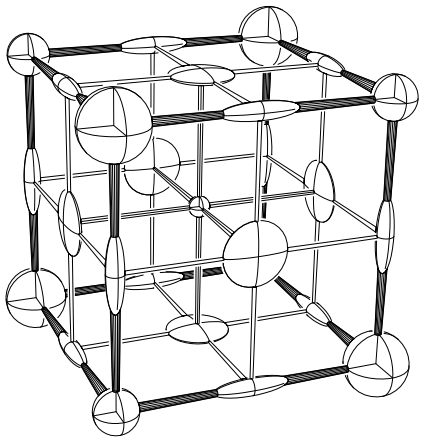

Figure 1.1. ORTEP critical net illustration of NaCl.

Fig. 1.2 shows the critical point (0=peak, 1=pass, etc.) locations in one octant of the unit cell for NaCl. A sodium ion is on the peak site in the lower right front, and a chloride ion is on the peak site in the lower right rear. The vectors in Fig. 1.2 point downhill, in a density sense, along the topologically unique paths of the critical net.

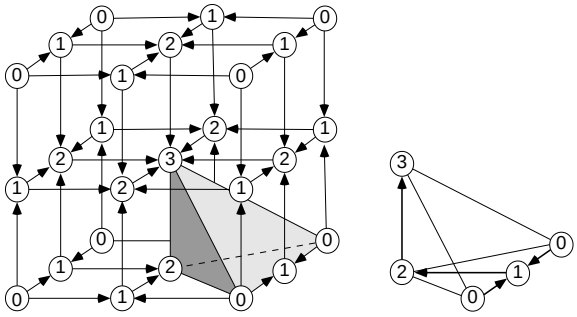

Figure 1.2. NaCl critical point network in one octant of the unit cell (left) and in an asymmetric unit of the unit cell (right).

NaCl crystals have the internal symmetry of space group $Fm\bar{3}m$, which is #225 in the ITCr.[1] The general position multiplicity within the unit cell is 192, which is the largest multiplicity possible in the space groups. Points on symmetry elements have smaller total unit cell occupancy, called the Wyckoff site multiplicity. Thus, there are 4 Na + 4 Cl peaks, 24 passes, 24 pales, and 8 pits in the unit cell. The shaded tetrahedron in Fig. 1.2 is an asymmetric unit (fundamental domain) of the unit cell, which occupies 1/24 of the volume shown and 1/192 of the unit cell volume.

1.4 Orbifolds

As Walt Kelly's philosophical comic-strip character Pogo might have said, "The trouble with symmetry is that it's too repetitious." Orbifolds remove all repetition; thus all space-group orbifolds will have roughly the same size and complexity (see Sect. 2.9), a situation that contrasts sharply with traditional crystallographic geometric drawings of space group symmetry as given in the ITCr.[1]

A crystallographic orbifold, Q, may be formally defined as the quotient space of a sphere, S, or Euclidean, E, space modulo a discrete crystallographic symmetry group, G (i.e., Q=K/G where K=S or E). G is one of the ordinary 32 2-D point groups if K is a 2-sphere, one of the 17 2-D plane groups if K is 2-Euclidean, or one of the 230 3-D space groups if K is 3-Euclidean. In the present discussion, we have no need to generalize into dimensions higher than three or to utilize hyperbolic orbifolds.

Another viewpoint is that an orbifold is a compact closed quotient space that results when all equivalent points are overlaid onto one parent point. In contrast to the orbifold's closed space, the crystal space is an open (infinite) Euclidean 3-space.

1.5 Orbifold for Space Group $Fm\bar{3}m$

Fig. 1.3-left shows the 3- and 4-fold rotational symmetry axes within an octant of the unit cell for $Fm\bar{3}m$, and Fig. 1.3-right shows the orbifold and its singular set using the orbifold nomenclature discussed in detail in Sect. 2. Briefly, the corner Wyckoff site (a), which has orbifold notation, 4'3'2', lies on 4-, 3-, and 2-fold axes running along its adjacent edges. All four faces contain mirrors, as denoted by the primes on the numbers and double lines in the drawing.

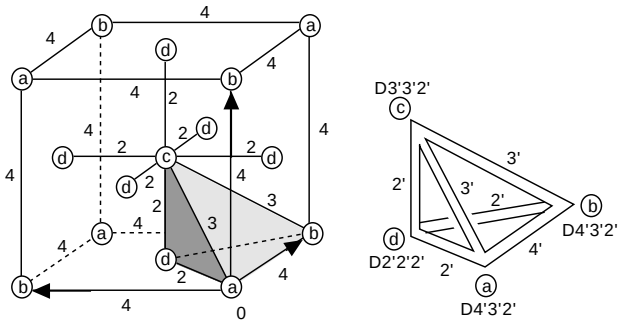

Figure 1.3. Euclidean 3-orbifold for space group $Fm\bar{3}m$.

The topological information for the tetrahedral Euclidean 3-orbifold of NaCl is expressed more economically in the skeletal drawing shown in Fig. 1.4-left, in which the viewpoint is directly above an apex of the tetrahedron. The mirror locations are indicated by the symbol

1' with the mirror for the bottom hidden face indicated by the cornered 1' over the tetrahedron. Every axis marked with a prime, such as 4', has to have two adjacent mirror planes and every corner point, such as 2'2'2' (inferred from the axes' intersections), has to have three adjacent mirror planes. Thus, we can interpret the skeletal tetrahedron details almost as easily as the double line mirror symbol drawing in Fig. 1.3.

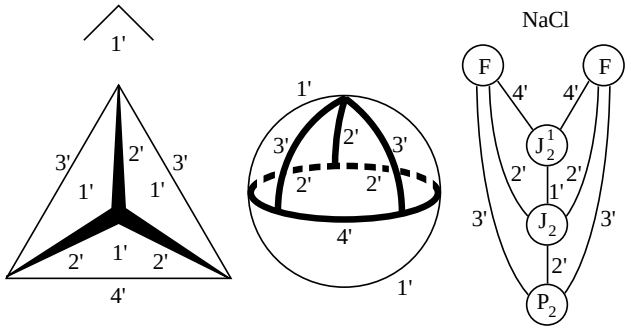

Figure 1.4. Fm$\bar{3}$m orbifold and NaCl critical-net-on-orbifold representations.

1.6 The Rubber Sheet World of Topology

An artist can exercise artistic liberties to emphasize desired features in a picture, but a topologist can and does exercise even more liberties in his rubber sheet world where any deformation is perfectly acceptable as long as you do not tear anything.[10] When topologists read the old warning label on computer punched cards, "do not fold, mutilate, or spindle," they probably only took the third item seriously. (The dictionary definition of spindle is to impale, thrust, or perforate on the spike of a spindle file.) Fig. 2.5 shows several examples of how a rectangle can be deformed in space and glued to itself to form a surface. In that spirit, it is perfectly acceptable to deform the tetrahedron into a sphere, as shown in the middle drawing of Fig. 1.4, and put the 3'3'2' dihedral corner and its attached 3' and 2' axes in the upper hemisphere. This makes the underlying topological space, a 3-ball, more readily apparent.

The Wyckoff site list for Fm$\bar{3}$m in the ITCr[1] tells us there are two mirrors, three 2' axes, one 3' axis, and one 4' axis. Yet in Fig. 1.4-middle, it appears these numbers should be 4, 3, 2, and 1, respectively. So what is going on? The answer is that a 3-fold axis can do strange and wondrous things simply because it is an odd-order axis, the only one in crystallography.

For example, in Fig. 1.3-left a single straight body-diagonal axis from a to b through c has two nonequivalent parts, ac and bc, while all even-ordered axis segments repeat themselves about an intersection of axes. Thus, what at first appears to be two different axes along the top edges of the asymmetric unit is in fact a single bent axis. A 3-fold axis can also bend a mirror around itself without breaking it. Thus in Fig. 1.4-middle, the three mirror segments in the upper hemisphere that are in contact with the 3-fold axis are simply different parts of the same mirror. All orbifold mirrors start and stop only at even ordered axes.

1.7 Linearized Critical Net for NaCl

By superimposing Fig. 1.2-right onto Fig. 1.3-right, we obtain a critical-net-on-orbifold representation, which is one of the main topics of our presentation. Again taking a few topological liberties, we can deform the whole critical-net-on-orbifold silvered 3-ball to arrange the peaks, passes, pales, and pits in sequence vertically down the page as shown in the right-hand drawing of Fig. 1.4. Thus, density decreases as you go down the page and we have literally mapped Euclidean 3-space to Euclidean 1-space, which is characteristic of Morse theory. This linearized critical-net-on-orbifold drawing still accurately portrays the Euclidean 3-orbifold and NaCl critical net information and is topologically correct. The symbols within the circles are lattice complex symbols discussed in Sect. 5.

This critical-net-on-orbifold drawing with the lattice complex information for each critical point site added provides an excellent summary of the structure's local and global topology, particularly if the Wyckoff site multiplicities are also recorded on the same drawing as shown in Sect. 4. The advantage that orbifolds and critical nets on orbifolds provide is a concise closed-space portrait of the topology for crystallographic groups and simple crystal structures, respectively.

2. Introduction to Orbifolds

Some elementary textbooks on geometric topology that we find useful include Barr,[10] McCarty,[11] Rolfsen,[12] and Kinsey[13] with Kinsey[13] the recommended introductory text. For more general mathematical topics, we use Ito.[14] The V-manifold of Satake[15] provided the first formal definition of what was later renamed orbifold and popularized widely by William Thurston. This concept was developed by Thurston into a major geometric topology discipline. Thurston's unpublished Princeton class notes of 1978 entitled "Three Dimensional Geometry and Topology," which is being expanded into a book manuscript of the same title,[16] and an article by Scott[17] constitute the main general references on orbifolds.

The first systematic study of crystallographic orbifolds was done by W. D. Dunbar[18] in his 1981 Princeton dissertation, carried out under Thurston, and in which he derived and illustrated the singular sets for the 65 polar space groups using oriented orbifolds. The parts of his dissertation related to the underlying hypersphere space S^3 were published in 1988.[19] The second major contribution to crystallographic orbifolds is the systematic development of orbifolds (both oriented and nonoriented) in Seifert fibered space in Bonahon and Siebenmann's unpublished manuscript.[20] Part of that manuscript related to

Euclidean 3-orbifolds, but omitting direct discussion of crystallography, was published in 1985.[21] A book on "Classical Tesselations and Three-Manifolds" by Montesinos[22] covers and expands certain aspects of Bonahon and Siebenmann's work.

A nomenclature system for 2-orbifolds was published by John H. Conway[23] of Princeton. Conway and Thurston have a nomenclature system[24] for noncubic Euclidean 3-orbifolds based on the lifting of 2-Euclidean orbifolds to form Seifert fibered spaces.

2.1 Types of Crystallographic Orbifolds

Three types of groups are at the foundation of general crystallography: point groups, plane groups, and space groups. Their respective orbifolds are spherical 2-orbifolds, Euclidean 2-orbifolds, and Euclidean 3-orbifolds. Sect. 2 is concerned with the first two types, and how they relate to the third.

Our main application of the spherical 2-orbifolds is relative to the Wyckoff sites and their symmetries which, in the case of a space group orbifold, become the components of its singular set. The singular set of an orbifold is the union of all the special Wyckoff sites in an asymmetric unit (fundamental domain) of the space group's unit cell. The symmetry of each Wyckoff site is called the isometry of that site (i.e., the part of the symmetry group which returns a point on that site to itself). The multiplicity for a Wyckoff site is the number of sites with that specific isometry within the unit cell and is the ratio of the isometry of the site to the order of the space group modulo the unit cell translations. The order of a space group itself is infinite.

2.2 Orbifolding Mechanics

Point groups are simply discrete symmetries about a point, limited crystallographically to the 2-, 3-, 4-, and 6-fold symmetries of cyclic, dihedral, tetrahedral, and octahedral groups. The 2-fold symmetries include mirror symmetry. Since it impossible to draw things on a point, a sphere about the point is used instead, and the intersections of the rotation axes and mirrors with the sphere are indicated in the point group drawings. There are also three kinds of mirror-free inversion centers symbolized $\bar{1}$, $\bar{4}$, and $\bar{3}$, with the latter two having 2- and 3-fold rotation axis subgroups, respectively.

Orbifold cone points are derived from a rotation axis that does not lie in a mirror, as illustrated in the top row of Fig 2.1. Orbifold corner points are derived from rotation axes that do lie in mirrors, as shown in the bottom half of Fig. 2.1. Orbifolding is simply the operation of wrapping, or folding in the case of mirrors, to superimpose all equivalent points. There are times when the orbifolding process itself is important since we may need to unfold the orbifold partially to obtain some other (covering) orbifold or to unfold it fully to obtain the original space (i.e., the universal cover). Covering orbifolds are related to the original orbifold as subgroups are related to groups (see Appendix). The universal cover[25] of all Euclidean n-orbifolds is Euclidean n-space and that for spherical n-orbifolds is the n-sphere.

Two topological surfaces, the 2-sphere and the 2-disk, are of fundamental importance and can be made by gluing cones or silvered edge disk fragments, respectively. A sphere may be constructed by gluing the non-silvered edges of two or more cones together, and a disk by gluing together the bases of two or more of the silvered edge disk fragments such as shown in Fig 2.1. We can also cut a hole out of the interior of a disk (i.e., the part away from the silvered edge) and glue in a cone base. Often it is advantageous to simply cut out an entire fundamental domain (the asymmetric unit of crystallography) and fold it up to match all edges (2-D case) or faces (3-D case).

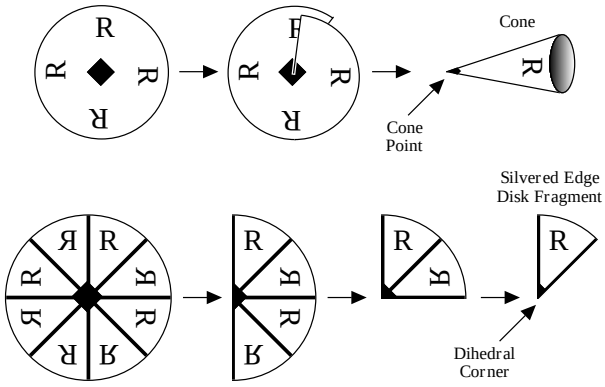

Figure 2.1. Formation of a cone and a disk fragment from 4-fold cyclic and 4-fold dihedral symmetries, respectively.

2.3 Deriving Point Group Orbifolds

There are seven main types of spherical 2-orbifolds, one for each column in Fig. 2.3, and we derive one orbifold of each type in Fig. 2.2, which has a stereographic projection of the point group in the top of each box and the corresponding orbifold in the bottom. We can drop the leading letters (i.e., S, D, and RP) of the orbifold symbol, as shown at the bottom of each box, without ambiguity. Fundamental domains for the point groups are shaded in Fig. 2.2. The thick solid lines denote mirrors; thin lines the edges of various regions; solid black diads and squares, 2- and $\underline{4}$-fold axes, respectively; a diad within an open square, a $\bar{4}$ inversion axis with the inversion point in the center of the sphere; and the thick dashed circle, an antipodal edge that is to be self-glued by a 180° rotation.

The orbifolds that contain a silvered-edge disk (symbol starts with D) with no cone points are simple to derive in that all we need to do is cut along the mirrors bounding the shaded area.

For other orbifolds, it is expedient to simply cut out the appropriate region of the sphere on which the point group acts and to glue the matching edges of the region

together to form a smaller surface. If the surface is a sphere, the symbol S is used. The gluing is fairly obvious for S44 where we are just forming a football, but S422 requires some explanation. Since each n-fold cone point divides the local environment into n parts, we must cut along great circles through 2-fold axes and along mutually normal great circles at the 4-fold axes. It does not matter how we choose the cut lines as long as they enclose a fundamental domain. Points along the cut edges leading away from the axes will be equivalent (by the symmetry of the axis) and are to be glued together. This creates some convenient envelope-type flaps, which we then bring together to form the 3-pointed pillow orbifold S422.

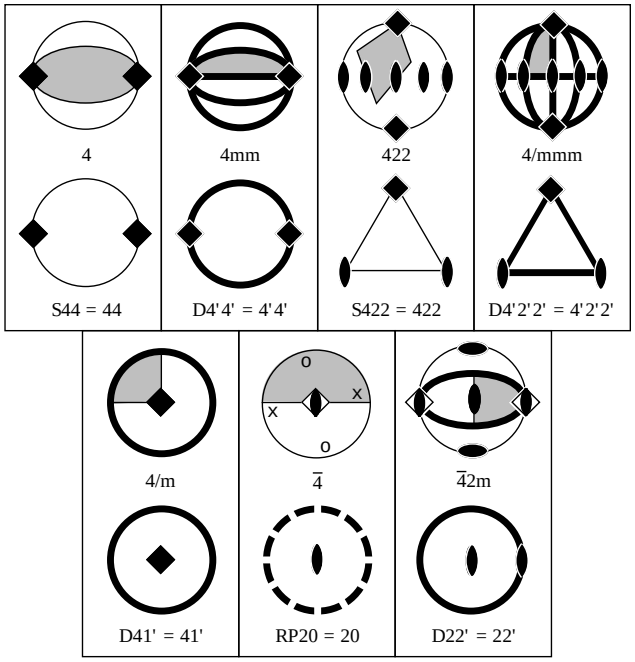

Figure 2.2. Derivation of spherical 2-orbifolds involving four-fold symmetry operations.

For the left-hand figure of the second row of Fig. 2.2, we first use the in-page mirror at the equator to bisect the sphere and form a hemisphere-shaped disk with silvered edge. We then mate the edges of the shaded 4-fold axis sector region and flatten the hemisphere to form a silvered edge disk, D41', with a 4-fold axis cone point.

In the middle figure of the second row, we are looking down a $\bar{4}$ axis which transforms point o → x → o → x → o with the o's on the upper hemisphere and the x's 90° away at the same latitude of the lower hemisphere. First we cut the sphere in half along the edge of the shaded area and close up the edges to form a new sphere with two cone points just as we would do for S22, which is not shown but which is analogous to S44. This new sphere has an inversion center that equates diametrically opposite points which we must now eliminate. We can cut along any great circle and discard one hemisphere to factor out this spherical inversion. The new cut edge has an antipodal relationship with equivalent points 180° apart. The cone point can be anywhere within or upon the boundary; but, of course, if it is on the boundary, it appears twice, 180° apart. In Fig. 2.2 it is shown centered within the boundary, but this is not a requirement as it was for D41', which has no antipodal edges. In the descriptive name RP20 for this orbifold, RP refers to the underlying surface, a real projective plane; 0 stands for the antipodal gluing on the disk; and 2 denotes the 2-fold cone point.

For the right-hand figure of the second row, we first cut the sphere in half vertically through the 2-fold axes and then cut along the mirrors to obtain the shaded area. We then have to fold around the vertical 2-fold axis on the left edge of the cut area to join the two mirror boundary components into a single continuous mirror boundary. Only the 2-fold axis of the $\bar{4}$ remains. In algebraic terms, the $\bar{4}$ of the point group is generated by one of the mirrors and a 180° rotation that doesn't intersect the mirror (i.e., by the 1' and the 2).

2.4 The 32 Point Group Orbifolds

Our proposed graphical representations illustrating the spherical 2-orbifolds for the 32 crystallographic point groups are shown in Fig. 2.3 arranged as 7 columns of topological families and 7 rows of crystallographic families. The columns are further partitioned into 15 group types designated by the symbols a,b,c for low cyclic; d,e,f for cyclic; g,h,i,j for dihedral; k,l,m for tetrahedral; and n,o for octahedral. This classification is patterned after that used by Bonahon and Siebenmann.[20] A tabulation of other names and notations for the series d-o is given by Conway.[23] Our "low cyclic" set a,b,c is not distinguished in the classification systems of others, and that row is not the usual one used in the crystallographic family tree; but these starter members in their series have special properties that become apparent when one constructs subgroup graphs (see Appendix) and crystallographic color groups.[26] We omit the icosahedral rotation groups since their 5-fold rotation axes are not crystallographic. The leading letter(s) of the orbifold symbols may be omitted without ambiguity.

Thick lines and circles in these spherical orbifold drawings represent silvered topological disks while thin lines and circles represent the apparent edges of 2-spheres. Dihedral corners are denoted by diads, triangles, squares, and hexagons lying in a thick line or circle. Cone points are denoted by the same symbols in a thin line or circle, or they are isolated within the drawing. These symbols are used instead of numbers for consistency with standard crystallographic symmetry drawings. The thick dashed circle designates an unmated projective plane edge, which has an antipodal gluing relationship (i.e. identical points occur half way around the edge).

An orbifold symbol is listed under each orbifold drawing with S, D, and RP denoting sphere, disk, and real projective plane, respectively. Mirrors are denoted by a

prime attached to a digit with 2', 3', 4', and 6' representing dihedral corners lying in mirror intersections. Mirrors without corners are denoted 1'. Cone points are given as 2, 3, 4, and 6.

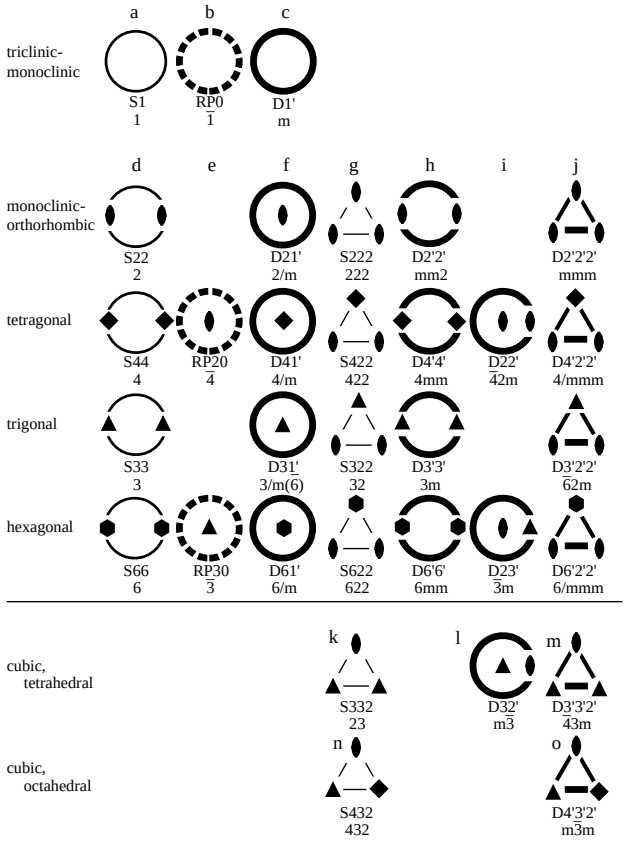

Figure 2.3. Spherical 2-orbifolds of the 32 crystallographic point groups.

The bottom symbol under each orbifold is the international short crystallographic notation for the point group from which the orbifold is derived, with overbars and m's denoting inversion centers and mirrors, respectively, and with 2, 3, 4, and 6 describing the order of rotation axes. All crystallographic symbols are based on group generators in a standardized geometrical setting with respect to coordinate system basis vectors and thus depend on which crystallographic family (i.e., row) is involved. In the Wyckoff site symmetry tables of the ITCr,[1] permutation of the symbol components may be encountered due to the setting of the point-group coordinate-system basis vectors relative to the unit-cell basis vectors (e.g., $\bar{6}$2m and $\bar{6}$m2). (The symbol $\bar{6}$ is a historical oddity of crystallographic notation and is algebraically identical to 3/m.)

2.5 Spherical 2-Orbifolds in Euclidean 3-Orbifold Singular Sets

The tetrahedral Euclidean 3-orbifold for NaCl shown in Fig. 1.3 is redrawn in Fig. 2.4 to portray how a mechanical draftsman might visualize the singular set of the NaCl orbifold based on the physical shape of the Fm$\bar{3}$m asymmetric unit in Fig. 1.3 and the topological details given in Fig. 2.3 for the component spherical 2-orbifolds.

The construction of singular sets (for Euclidean 3-orbifolds) from spherical 2-orbifolds might be considered as a game of orbifold space dominoes. You can only position a piece next to another piece with the same pattern on it. The rules of the game say that any two touching elements have to have a group/subgroup relationship.

Just as a sphere is the set of points at an arbitrarily small distance from an arbitrary point in 3-space, the 32 spherical 2-orbifolds described previously are models for the set of points at a small distance from an arbitrary point in a Euclidean 3-orbifold. There are 31 types of local singular environments and one type (S1) of nonsingular environment.

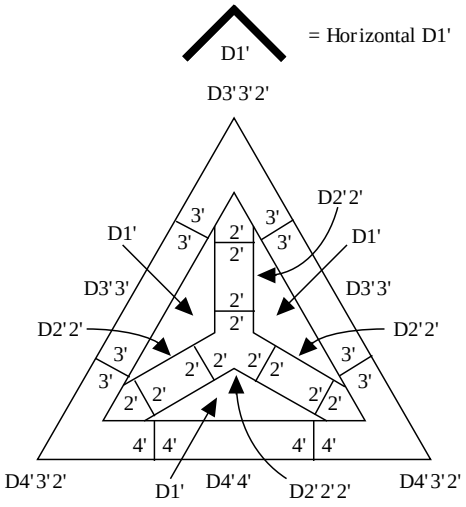

Figure 2.4. Fm$\bar{3}$m orbifold representation.

2.6 Surface Topology

Fig. 2.5 illustrates how rectangles when wrapped up to superimpose identical edges give rise to five basic topological surfaces present in the plane group orbifolds. The other two surfaces needed are the 2-sphere and 2-disk discussed in Sect. 2.2. The arrows on the edges of the rectangles indicate directional specific patterns that are to be superimposed and glued together. The projective plane and Klein bottle surface constructions are illustrated in two steps.

For the projective plane, the intermediate stage is a sphere with a hole in it that has an antipodal relationship along the gluing edge of the hole. The final step closes up the hole by puckering two opposite points down while the two other points 90° from the first pair are puckered up, forming a pinched end called a crosscap. The intermediate Klein bottle construction may be represented with an antipodal gluing relation on the single edge of a Möbius band, indicating that points half way along the single edge

are to be glued together. The dashed curves on both of these are related to glides as in Fig. 2.6.

The apparent self-intersection in the projective plane and Klein bottle is just a limitation of illustration techniques. The rules are that a manifold (or orbifold) can be embedded in whatever dimension Euclidean space is required. The projective plane and Klein bottle can be mapped into 4-dimensional Euclidean space with no self-intersections. For graphical simplicity, we will always draw the intermediate stage for these.

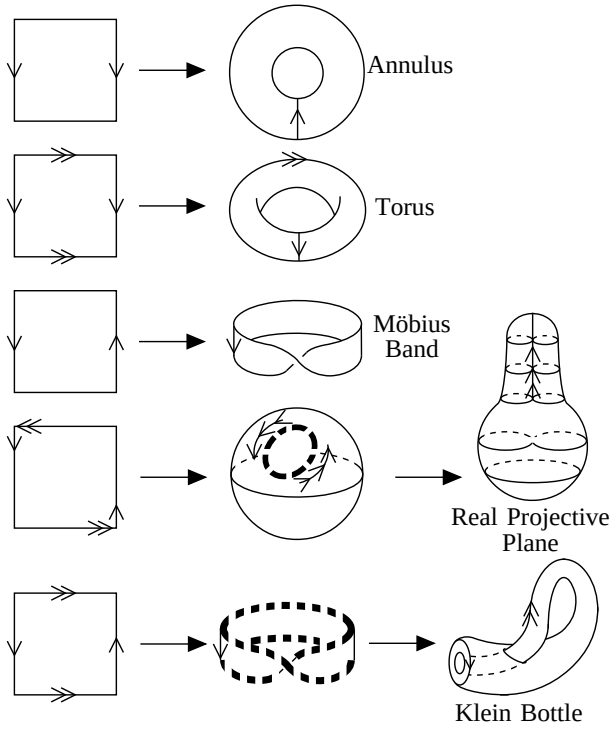

Figure 2.5. Formation of 5 topological surfaces from rectangles.

2.7 Plane Group Orbifolds

There are 17 plane groups defining the symmetry in all patterns that repeat by 2-dimensional lattice translations in Euclidean 2-space. We will derive the 17 Euclidean 2-orbifolds directly from standard crystallographic plane group drawings. The graphic conventions of Sect. 2.4 are followed in this section also.

In Fig. 2.6. the heaviest lines indicate where folding takes place, and the shaded lines are where cutting is done. After cutting, symmetry equivalent edges are pasted together to form the Euclidean 2-orbifolds at the bottom of each box.

The notation under the crystallographic drawing is the standard plane group name and that under the orbifold drawing is our notation for the Euclidean 2-orbifold. “Möbius” denotes a Möbius band with one silvered edge, and “Annulus” denotes an annulus with two silvered edges. S2222, S333, etc. are called pillow orbifolds and have the constraint that for Sijk..., (i-1)/i + (j-1)/j + (k-1)/k + ... = 2. Heavy lines and circles indicate mirrors, and a heavy dashed circle, arising from a glide, signifies a projective plane antipodal gluing edge. Primed numbers indicate the corresponding rotation axis lies in a mirror forming a dihedral corner, and unprimed numbers indicate cone points.

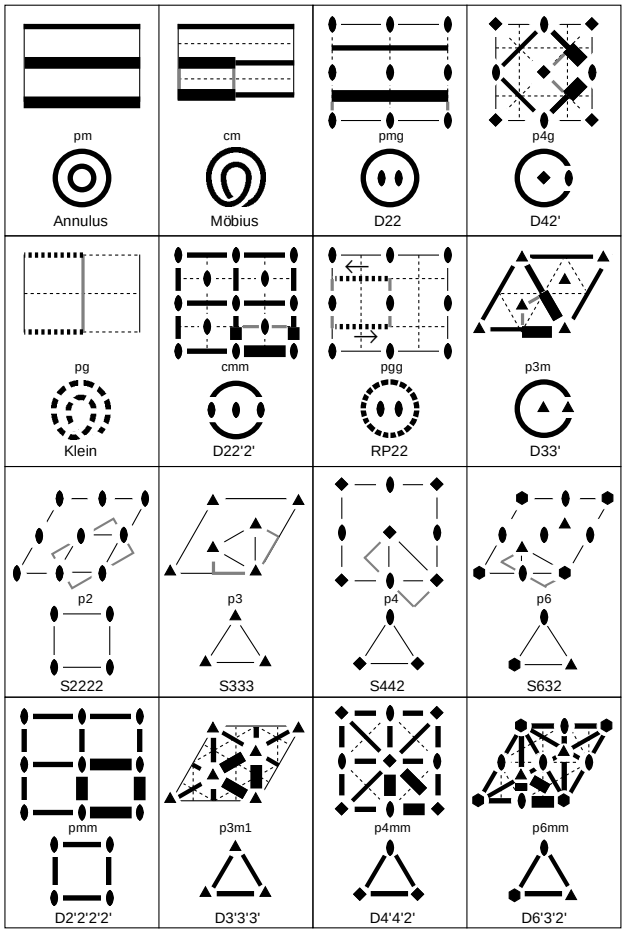

Figure 2.6. Derivation of the plane group Euclidean 2-orbifolds.
Plane group p1, a torus, is not shown.

The orbifolds in the third row of boxes are derived by using straight line cuts through 2-fold axes and appropriate angular cuts at other axes to leave some flaps which are then glued together to produce the 4- and 3-cornered pillow spherical orbifolds. The orbifolds on row four simply require cutting along the heaviest lines in the plane group drawings. The remaining orbifolds (rows one and two) are derived by cutting along the heaviest lines and along appropriate angles through the single axis pointed to by vectors perpendicular to the ends of the heaviest lines, then closing up the cut edges through the axis to form a complete silvered boundary.

The annulus and Möbius band in row one are derived from plane groups pm and cm by first cutting out an asymmetric unit bounded by those portions of the mirrors denoted by heaviest lines and matching the ends together. The p1 (torus) asymmetric unit requires the whole unit cell, as is illustrated only in Fig. 2.5.

For the projective plane orbifold, RP22, 1/4 of the unit cell is required for the asymmetric unit. At first we choose an asymmetric unit with a 2-fold axis on each corner and fold up as indicated in Fig 2.5. This places all four 2-fold axes on the dashed circle where the antipodal relationship holds so that it looks pictorially like the D2'2'2'2' symbol with the dashed boundary replacing the mirror boundary. However, we then note that by moving the asymmetric unit one quarter cell in either the x or y direction, there are now two 2-fold axes centered on opposite sides of the asymmetric unit as shown in Fig. 2.6. Folding about these 2-fold axes positions them in the interior of the orbifold as shown in the RP22 orbifold figure and there is still an antipodal relationship along the gluing edge. Thus, we can push two nonequivalent pairs of equivalent axes off the boundary to get two nonequivalent axes in the interior of the projective plane orbifold, or vice-versa, while still maintaining the antipodal gluing edge relationship. Only the projective plane has this amazing "sliding" gluing edge property. The Klein bottle is related to the projective plane in that they both have an antipodal gluing edge. However, the antipodal edge of the Klein bottle is on a Möbius band while that of the projective plane is on a disk.

2.8 Lifting Plane Group Orbifolds to Space Group Orbifolds

The ITCr[1] lists the projection symmetry plane groups along three special axes for each space group. Different crystallographic families have different unique projection axes. For example a cubic space groups has special projected symmetries along (001), (111), and (011) while the orthorhombic special directions are (100), (010), and (001). Space group nomenclature used by crystallographers also follows this trend by listing generators for each unique axis with nontrivial projection symmetry.

Much of the orbifold topology literature (e.g., Bonahon and Siebenmann[21]) uses a Euclidean 2-orbifold as the base orbifold, which is lifted into a Euclidean 3-orbifold using the Seifert fibered space approach[27] while keeping track of how the fibers (or stratifications) flow in the lifting process. This works only for the 194 non-cubic space groups since the body-diagonal 3-fold symmetry axes of the 36 cubic space group violate the Seifert fibered space postulates. However, there are some work-around methods using 3-fold covers that let you derive the cubic Euclidean 3-orbifolds from their corresponding orthorhombic Euclidean 3-orbifold covers.

Many space groups have underlying space S^3 (3-sphere) and are relatively easy to draw. Fig. 2.7 illustrates five different fibrations of Euclidean 3-orbifolds over the 2-orbifold D4'4'2', corresponding to space groups I422 (#97), P422 (#89), $P4_222$ (#93), $I4_122$ (#98) and $P4_122$ (#91), which all originate from point group 422. The base Euclidean 2-orbifold is in the middle of Fig. 2.7 and the Euclidean 3-orbifolds are in the top halves of the boxes with singular set drawings in the bottom half. The numbers of independent Wyckoff sets (i.e., spherical 2-orbifolds) are shown in parentheses in the smaller boxes.

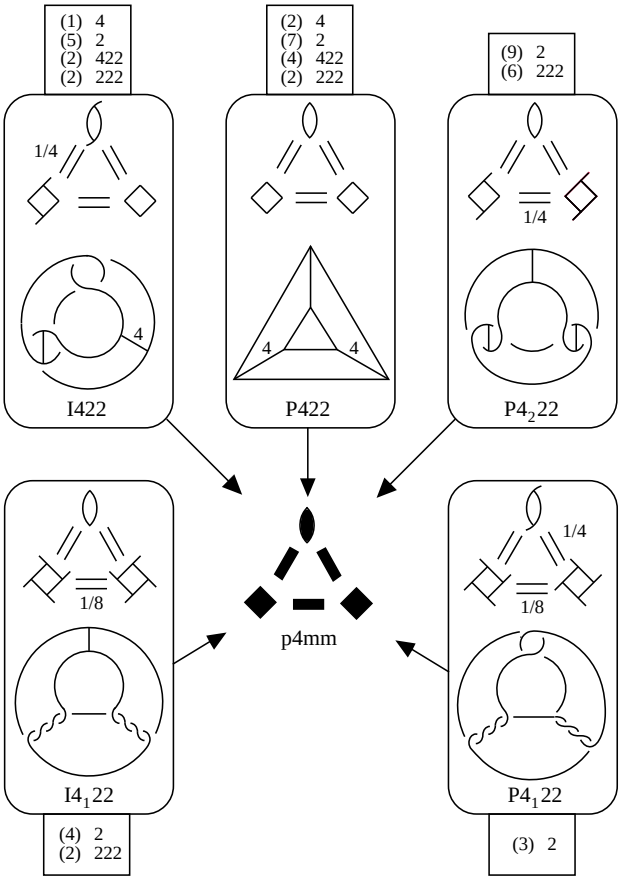

Figure 2.7. Space group orbifolds from point group 422 and plane group p4mm.

Note the correspondence between the 3-orbifold symbol and the singular set drawing. In P422 we are looking down a trigonal prism fundamental domain with vertical 4-fold axes along two edges and 2-fold axes along the seven other edges and there are six trivalent intersections at the corners. In $I4_122$ the two 4-fold axes become 4-fold screws, one right-handed and one left-handed, Also note that the twisted pair of 2-fold axes in the orbifold has the opposite handedness to that indicated by the symmetry symbol. In $P4_222$ the 4_2 axes become 2-fold screw axes with 2-fold axis struts across the 2-screw loops since a 4_2 axis contains both a 2-fold axis and a 2-fold screw subgroup. The $P4_122$ singular set diagram is called a link since there are no connections among the three 2-fold axes.

It may be instructive to check the close correspondence between the symbols in Fig. 2.7 and the ITCr[1] space group symmetry drawings. The fractions over certain edges in Fig. 2.7 denote distance along the viewing direction. Thus, a 2-fold screw axis raises or lowers the in-plane 2-fold axes by 1/4 and a 4-fold screw axis raises or lowers them by 1/8, depending on the screw handedness.

We do not currently use this lifted 2-orbifold method since we now prefer to construct orbifolds from the full 3-dimensional fundamental domain, which provides a procedure valid for all space groups including the cubics. However, most of the orbifold literature does use some variety of the lifted base orbifold convention and the existing 3-orbifold nomenclature is based on it. The reason is that the topological classification of 2-manifolds (surfaces) is classical and well understood, but 3-manifold classification is still incomplete.

2.9 Orbifolds from Polar Space Groups

There are 65 polar (i.e., orientable) space groups. The 65 orientable Euclidean 3-orbifolds are derived and illustrated in Dunbar's dissertation.[18] Of the 20 polar space groups with cyclic point groups (1, 2, 3, 4, and 6), 12 have orbifolds with underlying space $S^2\times S^1$, 1 has underlying space $S^1\times S^1\times S^1$ (torus) and the remaining 7 are Euclidean 3-manifolds with empty singular sets which are flat Riemannian manifolds.[28] Of the 45 polar space groups with other point groups (i.e., 222, 422, 312, 321, 32, 622, 23, and 432), 4 have orbifolds with underlying spaces RP^3, 1 with $RP^3\#RP^3$ (# denotes a connected sum), 4 with lens spaces,[12] 1 with a Euclidean manifold,[28] and 35 with S^3.

Fig. 2.8 shows the singular sets for all 35 Euclidean 3-orbifolds that have S^3 as their underlying topological space. The ten orbifolds in the bottom two rows have no vertices in their singular sets and have from one to four closed loops. The single-loop example in the last column of the last row is a topological knot and the remaining nine are links.[12] The remaining 25 orbifolds in Fig. 2.8 have either planar graph (first four of the third row) or knotted graph singular sets. There are 12 cubic orientable orbifolds (the ten in the top two rows and one each in the bottom two rows). The first three of the first row are tetrahedral orbifolds as the one in Fig. 2.4.

An interesting feature of Fig 2.8 is that all the orbifolds have roughly the same complexity, which is independent of the parent crystallographic space group families. This is true of all 230 crystallographic orbifolds.

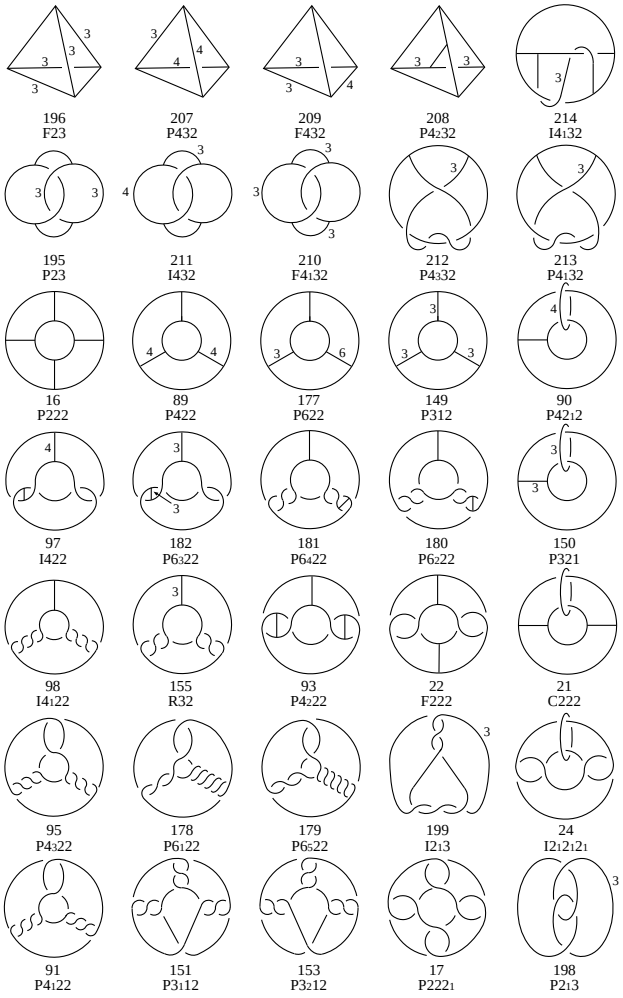

Figure 2.8. Singular sets for all 35 Euclidean 3-orbifolds that have S^3 as their underlying topological space.

tions on a frequent basis. The density may be electron density or nucleus thermal motion density depending on the type of Bragg diffraction intensities measured for the crystal structure determination, x-ray or neutron.

In calculated crystallographic density maps, the thermal motion smearing factor most often used for an individual atom is the 3-dimensional normal probability density function, which is also called the Gaussian density function. The density function for an individual atom may be either isotropic with spherical equidensity contours or anisotropic with ellipsoidal equidensity contours, depending on the site symmetry[29] for the atom within the crystal. With neutron diffraction, there is no extra smearing due to the electron orbitals within an atom since neutrons are primarily scattered by the point-like nucleus of an atom and not by the electrons. For x-rays the situation is reversed and an atomic form factor is required in addition to the thermal motion density function.

3. Introduction to Critical Nets

3.1 Crystallographic Morse Function

Our model for the crystallographic Morse function is based on concepts familiar to crystallographers who must deal with crystallographic three-dimensional density func-

The Gaussian density function has tails that extend to infinity; hence if we assume all atoms are positive scatterers and there is no experimental error or data truncation (i.e., a calculated map without data truncation), the summed density function within the crystal never goes to zero. Thus, the tails of the thermal motion density functions for all the atoms in the entire crystal overlap, but the density between atoms is considerably less than the density at the atomic sites. This idealized global density function is the basic model on which we do critical point analysis. We completely ignore all quantum chemistry electron orbital effects. A topological interpretation of the quantum chemistry effects is given in Bader.[9]

Mildly overlapping Gaussian density functions in a space group provide a smooth function that is well suited for Morse theory. The atom centroid (mean or first moment of the normal probability density function) is to a first approximation at a mode (extremum) of the density; thus peak positions correspond with atom positions. Our working hypothesis is that all valid real stable crystal structures are Morse functions, which by definition have no degenerate critical points.

3.2 Morse Theory

The first application of Morse theory to crystal physics was by van Hove,[30] who showed that certain singularities in lattice dynamics originate from crystallographic symmetry. Morse theory has a nice qualitative treatment in El'sgol'c.[5] The standard mathematical reference for Morse theory is Milnor;[3] but our application, which involves equivariant (i.e., group orbit compatible) topology,[31] seems to require the Morse theory treatment by Goresky and MacPherson.[4]

Some formal results concerning Morse functions on orbifolds are starting to appear in the mathematical preprint literature (e.g., Lerman and Tolman[32]), but these are primarily based on symplectic rather than Euclidean geometry (cf., Kirwan[33]). In our case we know the Euclidean space analogues of our Morse functions on orbifolds are well behaved so we can always unfold back to Euclidean 3-space for detailed analysis when necessary.

3.3 D-Symbol Tiling Alternative

A technique related to our Morse function critical net approach is the Delaney-Dress D-symbols method used by Dress, Huson, and Molnár[34] and Molnár.[35] That method uses topological space tiling, which is currently more automated but perhaps less general in its crystallographic applicability than ours. The space tiles are based on four types of special positions interpretable as vertices, edges, faces, and centers of polyhedra. The method produces a decomposition of each polyhedron into component simplex tetrahedra. The critical net and the D-symbol approaches lead to identical results in seven of the nine families where their method applies.

Their "special rhombohedral"[34] tiling example, which is not a Morse function, is actually body-centered cubic based on vertex (atom) positions as illustrated later in Fig. 3.4 and Fig. 4.2. Their "covered rhombohedron"[34] is not a Morse function either since there are not enough pales to fill all the faces. As mentioned previously, our working hypothesis is that all real crystal structures are Morse functions (i.e., they have no degenerate critical points). Degenerate critical points suggest structural instability, which should be present only during dynamic processes such as phase transitions.

The D-symbol computational method was also used to derive orbifold singular set components and their graph connectivity but not the full space group orbifolds.[36] The combinatorial graph connectivity distinguishes 175 of the 219 affine space group types. The remainder of the 219 may be distinguished using abelian invariants.

3.4 Chemical Faces and Cages

The following chemically-oriented nomenclature allows structural chemistry intuition to be used more easily in interpretation of critical net drawings. First, we note that peaks always represent atoms and passes sometimes, but not always, represent chemical bonds. We define a "chemical face" in a critical net as a (generally nonplanar) disk containing one pale bounded by a graph circuit containing alternating peak and pass nodes with edges along their interconnecting separatrices. A "chemical cage" is defined as a configuration of chemical faces that encloses one pit. A chemical cage is a convex polyhedron only in the simplest cases such as the primitive cubic critical net.

A detailed list of our observed critical net properties is given in Sect. 3.10, but in general, the universal geometric pattern in critical nets is: (a) the three or more passes attached to a pale will be approximately coplanar with the pale, and the approximately plane-normal critical-net connection at the pale will go to two pits, one on each side; and (b) the three or more pales attached to a pass will be approximately coplanar with the pass, and the approximately plane-normal critical-net connection at the pass will go to two peaks, one on each side. It is advisable to forgo all the distance and angle metric local detail so characteristic of structural crystallography while doing crystallographic topology.

3.5 Diamond Critical Net

Fig. 3.1 is a drawing of one chemical cage and the neighboring pits for the diamond structure (space group Fd3m). It has non-planar chemical faces and thus the diamond chemical cage is not a convex polyhedron. In diamond, there is one unique tetrahedral chemical cage with chair-shaped chemical faces.

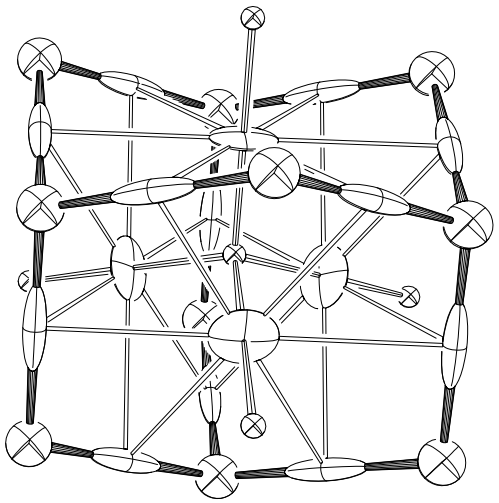

Figure 3.1. Critical net illustration of diamond.

3.6 Graphite Critical Net

The peak, pass, pale, and pit critical points for the $P6_3/mmc$ graphite structure, illustrated in Fig. 3.2, are at Wyckoff sites b+c, a+h, d+g, and f (with z = -.03), respectively. Two symmetry equivalent chemical cages are shown in the graphite illustration to clarify the packing arrangement. If one is conditioned by training to always look for convex polyhedra with atoms at the vertices, the single unique tetrahedral chemical cage with one planar and three chair-shaped chemical faces might mistakenly be interpreted as a hexagonal prism polyhedron with three of the vertex atoms pinched together at one end of the prism. The disturbing feature of the prism interpretation is the existence of a pseudo face of zero area in the pinched end of the prism. We call this the "graphite paradox." All the graphite chemical bonding is in the flat six-membered chemical face of the tetrahedron.

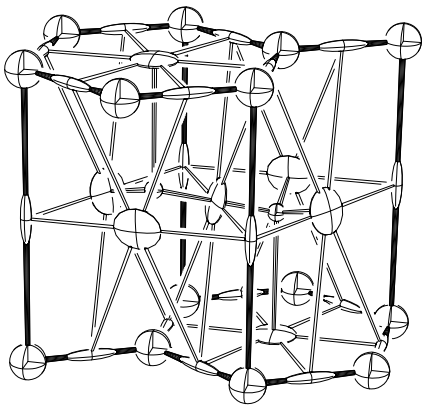

Figure 3.2. Critical net illustration of graphite.

3.7 Hexagonal Diamond Critical Net

In addition to the cubic diamond and hexagonal graphite structures shown above, there is a third simple carbon structure called hexagonal diamond,[37] which has the same space group as graphite ($P6_3/mmc$). Its critical net is illustrated in Fig. 3.3. This structure is not widely known since the material is hard to find in natural sources and is difficult to synthesize. It has both boat- and chair-shaped six-membered rings and two different chemical cages. The graphite and hexagonal diamond critical nets may seem quite different, but they are topologically related through duality as shown in Sect. 5. and Fig. 5.4.

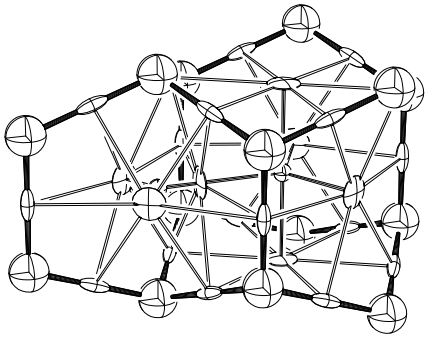

Figure 3.3. Critical net illustration of hexagonal diamond.

3.8 Body-Centered Cubic (BCC) Critical Net

Using the bcc structure of space group $Im\bar{3}m$ as a template, binary compounds can also be fitted into the same basic structure. For example, the $Fd\bar{3}m$ space group can accommodate two different atoms on the two $\bar{4}3m$ sites as illustrated in Fig. 3.4, which shows five chemical cages. The lattice complex splitting equation I_2=D+D" given in Sect. 5.3 tells us that two equal atoms on Wyckoff sites a and b of $Fd\bar{3}m$ are equivalent to one atom on site a of $Im\bar{3}m$ when the unit cell parameters of the former are double those of the latter. This bcc derivative is our Morse function alternative to the special rhombohedron tiling of Dress, Huson and Molnár.[34]

Bcc is the ultimate example of warped chemical faces. There are four puckered chemical faces, each containing four peaks and four bonds in a chemical cage. The pales in the four faces have a square planar arrangement about the pit while the 6 peaks are octahedral about the pit because of the vertex sharing arrangement.

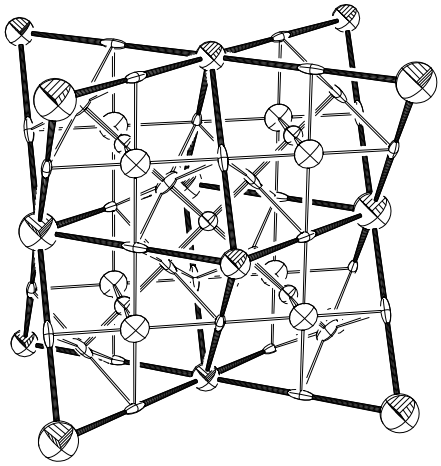

Figure 3.4. Critical net illustration of body-centered cubic derivative.

3.9 Basic Beryllium Acetate Critical Net

The cubic organometallic compound basic beryllium acetate [$Be_4O(CH_3CO_2)_6$, $Fd\bar{3}$, a=15.744 Å, Z=8] has eight atoms in the asymmetric unit and orientationally disordered methyl groups.[38] A molecular compound such as this can display a rather complex critical net that is difficult to solve using simple trial and error methods and the disorder increases the complexity. Fig. 3.5 illustrates a key portion of the network which has a pit on a $\bar{3}$ center connecting six pales centered within hexagonal rings of two neighboring molecules. The opposite sides of the pales connect to symmetry equivalent $\bar{3}$ centers. The oxygen atom spheres in Fig. 3.5 are slightly larger than those for other atoms, and the beryllium atom spheres have a shaded octant, For graphics clarity, hydrogen atoms have been omitted from the methyl groups, and only half of each molecule is shown.

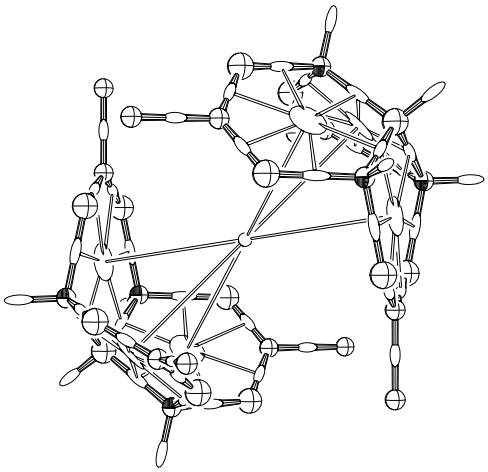

Figure 3.5. Part of critical net for basic beryllium acetate.

3.10 Critical Net Characteristics

Below are some definitive characteristics that are useful for finding and analyzing critical nets for very simple structures. For more complex structures, critical point positions and the canonical paths joining them can be determined numerically from calculated global Gaussian thermal motion density maps based only on given atomic (i.e., peak) positions. The author's ORCRIT program for protein electron density map interpretation,[39] originally written in 1977, could be modified for that purpose. High precision experimental electron density maps from x-ray data and charge density maps calculated by *ab initio* quantum chemistry programs are more complicated than those considered here because of the possible addition of new critical points caused by bonding electrons etc.

- Peaks are at atom positions.
- Pits are as far from all adjacent peaks as possible, but there is always an ancillary steepest gradient path leading directly from the peak to each adjacent pit.
- A pass lies between two adjacent peaks.
- A pale lies between two adjacent pits.
- A pale lies on or close to the plane perpendicular to each adjacent pass' unique axis (i.e., the symmetric cross section of the cigar-shaped pass).
- A pass lies on or close to the plane perpendicular to each adjacent pale's unique axis (i.e., the plane of the pancake-shaped pale).
- Each fixed point Wyckoff position of the space group must contain a critical point of the crystal structure.
- Wyckoff positions with the cubic site symmetries for tetrahedral (23, $m\bar{3}$ and $\bar{4}3m$) and octahedral (432 and $m\bar{3}m$) point groups can only accommodate peaks or pits, not passes nor pales, because of their body-diagonal 3-fold axes. All of the other 32 - 5 = 27 possible point group site symmetries in a space group can accommodate any of the four critical points.
- The critical net is composed of interconnected "twisted Hs" with pairs of peaks and pits at the ends of the two inclined non-parallel uprights and a pass and a pale at the ends of the horizontal connector, which is the shortest vector between the two non-parallel uprights.
- The twisted-H torsion angle about the pass-pale vector ranges from about 45° (e.g., bcc) to 90° (e.g., simple cubic).
- Critical nets always maintain a peak-pass-pale-pit vs. pit-pale-pass-peak duality, that is the naming of the critical point sites can be reversed to produce a new valid Morse function. For example, the body-centered cubic structure with unit cell critical point counts of 2 peaks, 8 passes, 12 pales, and 6 pits, represented simply as (2,8,12,6) and which is the lattice complex "I", forms an "inverted" dual structure (6,12,8,2), lattice complex "J*", if atoms are removed from the bcc

peak sites and new atoms positioned at the bcc pit sites.

- The number of peaks, passes, pales, and pits in a unit cell (i.e., in a 3-torus $S^1 \times S^1 \times S^1$) obeys the Euler-Poincare relationship for Euclidean space, i.e., peaks - passes + pales - pits = 0, and the following Morse inequalities:

  pits ≥ 1
  peaks ≥ 1
  pales - pits ≥ 2
  passes - peaks ≥ 2
  passes - pales + pits ≥ 1
  pales - passes + peaks ≥ 1

- The inequalities are too weak to be of much value in practice; thus, there is a definite need for much stronger inequalities that incorporate space group specific invariants based on equivariant topology and can be applied to the wrapped-up asymmetric unit (i.e., orbifold) rather than the wrapped-up unit cell (i.e., 3-torus cover).
- The total number of critical points of a given type belonging to an asymmetric unit (fundamental domain) of a crystallographic unit cell can be calculated by dividing the sum of Wyckoff site multiplicities for all sites occupied by critical points of that type by the Wyckoff site multiplicity for the general position site. For simple high symmetry structures, this number is often less than one.
- Since the Betti numbers for the 3-torus are 1,3,3,1, the minimum number of critical points possible in a crystallographic unit cell is 8, (i.e., 1,3,3,1 in $P\bar{1}$ with critical points on the 8 inversion centers). Betti numbers are topological invariants used in the derivation of the Morse inequalities.[2,3,5]
- The inequalities are still of little practical value; thus, there is a definite need for much stronger inequalities that incorporate space group specific invariants based on equivariant topology and can be applied to the wrapped-up asymmetric unit (i.e., orbifold) rather than the wrapped-up unit cell (i.e., 3-torus).

4. Critical Nets on Orbifolds

In Sect 3. we saw that critical net drawings can become rather complex even for very simple examples such as the body-centered cubic (bcc) structure. In the present section, we introduce critical nets on orbifolds, which reduce both the graphical and interpretation complexity associated with critical nets while including valuable space group topology information as well.

4.1 Body-Centered Cubic Orbifold

The orbifold for $Im\bar{3}m$, the parent space group for bcc structures, is derived from the fundamental domain shown in the lower left of Fig. 4.1. The space group coordinates for the vertices of the fundamental domain are given in parentheses as fractions of the unit cell lengths. The arrows denote the down density critical net paths leading from the peak at (a) to the pit at (b). Wyckoff identification letters (a-k) are shown on the asymmetric unit drawing, and the ITCr[1] information on most of those Wyckoff sites is listed in the columns labeled "Wyckoff Set" in the middle of the figure. The tetrahedral fundamental domain has three sides bounded with the top (k) and bottom (j) mirrors with (k) bridged over the 3-fold axis as described in Sect. 1.6, but the fourth side is open (unbounded) with a 2-fold axis (i) extending from one corner of the open end (c) to the center (d) of the opposite face, which contains another 2-fold axis (g).

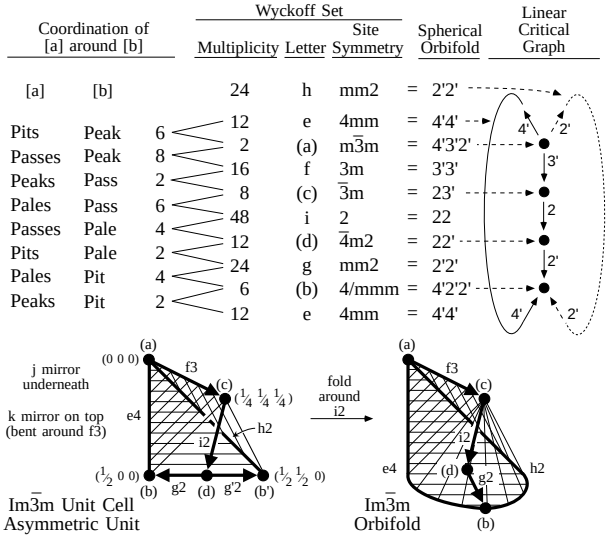

Figure 4.1. Construction of $Im\bar{3}m$ orbifold from asymmetric unit and superimposition of body-centered cubic lattice complex to form linear critical graph.

Visualize the tetrahedral asymmetric unit as a single-pole pup tent, covered by a silvered rubber reflective sheet, with a support pole (i) in the entrance. A horizontal "threshold" pole (g) with a hinge in the middle (d) lies across the front of the tent floor with the hinge attached to the bottom of the support pole. To close the tent, we grab the two corners of the rubber sheets (j and k) at the two ends (b) and (b') of the hinged threshold pole (g) and bring them together stretching the extensible and flexible tent floor poles (e) and (h) in the process. We then zipper the edges of the sheet (k) together to form the bounded orbifold shown in the lower right drawing of Fig. 4.1.

The underlying topological space of this 3-orbifold is a 3-ball. Using the notation in Fig. 2.3, the orbifold has two singular points of type j, 4'3'2' at (a) and 4'2'2' at (b), and two singular points of type i, 23' at (c) and 22' at (d).

4.2 Linearized Critical Nets on Orbifolds

Critical nets are actually Morse functions that are defined in terms of a mathematical mapping from Euclidean 3-space to Euclidean 1-space (i.e., a single valued 3-dimensional function). Taking this requirement literally, we deform the orbifold so that the Euclidean 1-space of density is vertical in the page (i.e., peak height > pass height > pale height > pit height). This adds a welcome constraint to the drawing of orbifolds that in general have no inherent topological constraints to guide the illustrator. The topologist would probably tend to draw it as a solid sphere, but we are not violating any topological principles in forming the linearized critical net on orbifold (i.e., linear critical graph) shown at the top of Fig. 4.1.

The multiplicity for each Wyckoff site is given as a column in the table and the preceding column shows the integer ratios of the multiplicities in adjacent rows, which are by design the adjacent elements in the critical net graph. These ratios tell us the coordination numbers of critical net components around other critical net components, thus summarizing much of the structural topology information you would obtain by examining ORTEP-III critical net stereo drawings or calculating and evaluating long tables of intercomponent distances and angles. Note the abbreviated orbifold critical set notation in the linear critical graph of Fig. 4.1 where 3'3' becomes 3', and stationary points such as 4'3'2' are denoted by the labels on the lines intersecting at that point.

4.3 Resolution of the Critical Net Versus Tiling Discrepancy

The coordination numbers also provide a method for applying topological constraints in that there must be exactly two peaks around a pass and two pits around a pale. This particular combinatorial constraint holds for the tiling approach of Dress, Huson, and Molnár[34] as well as for our critical net Morse function approach. Fig. 4.2 shows two solutions satisfying that constraint based on the orbifold topology for space group Fd$\bar{3}$m with atoms (i.e., tiling vertices in the Dress approach, peaks in the critical net approach) on the two $\bar{4}$3m sites of Fd$\bar{3}$m. Fig. 4.2 compares the two configurations assuming both are linearized critical nets on the Fd$\bar{3}$m orbifold. The columns of numbers are sums of Wyckoff set multiplicities for each level of the critical net and integer ratios of neighboring rows. Only the connections between adjacent levels are summed. An ORTEP drawing of the configuration labeled bcc derivative is shown in Fig. 3.4. A similar drawing cannot be made for the special rhombohedral tiling given by the second configuration since the two pales are far from collinear with the pit.

What's going on here? First, we note that the left configuration has seven nodes while the right has only six, but the six in common are on the same Wyckoff sites and point positions. We then note that on the orbifold drawing, in the lower right of the figure, the h2 axis lies directly between the (e) and (f) sites. Since a separatrix line can never traverse more than one isometry zone (i.e. Wyckoff site zone), there has to be another critical point at point (h). According to the special rhombohedral indexing, this point would have to be a degenerate critical point with a cubic (triple point) algebraic dependence rather than quadratic along the (e) to (f) vector since the density is heading downhill along that vector. We can always decompose a degenerate critical point into several nondegenerate critical points, but then we would be in trouble satisfying the Euler-Poincare relationship described in Sect. 3.10. The obviously related (c) and (d) Wyckoff sites must be assigned to the same Morse function levels, which then produces the correct configuration shown in the left-hand drawing.

In other situations, missed critical points may make one of the critical points found appear to be degenerate. In our experience to date, a critical net that is not a Morse function has always been traceable to misindexing caused by the omission of valid critical points. Once the peak positions have been assigned by positioning atoms and assigning their Gaussian thermal motion parameters, the rest of the critical net is fixed; it is just a case of determining what it is. In the simple structures we are discussing in this treatment, the thermal motion probability density is either constrained by symmetry to be isotropic or assumed to be isotropic and in any case has little effect on critical net details. Thus we omit smearing functions from the discussion other than to say they are isotropic, Gaussian, and mildly overlapping.

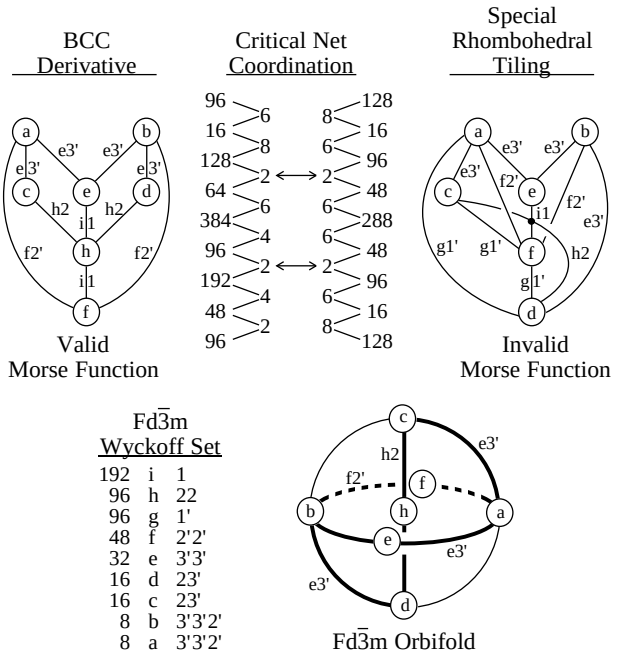

Figure 4.2. Comparison of critical net and tiling results.

5. Lattice Complexes on Critical Nets on Orbifolds

Critical nets on orbifolds, as presented in Sect. 4, provide a wealth of local topology information about the parent space group and simple structures on that space group. The global topology information is also there, encoded in the macrodetails of the combined critical net graph and orbifold, but sometimes we need a more specific summary of the global picture. A simple example concerns the difference between face centered cubic (fcc) and hexagonal closest packing (hcp) which have identical substructures as indicated by the coordination vector as shown in Figs. 5.2 and 5.4. Lattice complexes are convenient for the next step up past the coordination vector. In fact, the fcc and hcp configurations have their own lattice complex symbols F and E, respectively.

5.1 Lattice Complex Background

Lattice complexes have a 77 year history in crystallography. We find much of the literature on lattice complexes more complex than we need for our application, but there is a well written paper[40] that describes the basics we use. Once those basics are understood, certain key tabulations in Fischer, Burzlaff, Hellner, and Donnay;[41] Koch;[42] and Fischer and Koch[43] become useful. The definition given in the most recent reference[43] is that a lattice complex is the set of all point configurations that may be generated within one type of Wyckoff set. Hellner's definition[40] is that a lattice complex is an arrangement of equivalent points (or equipoints) that are related by space group symmetry operations, including lattice translations. Example applications of lattice complexes are given by Hellner, Koch, and Reinhardt.[44]

Lattice complexes are configurations of points that recur at least once but usually repeatedly throughout the family of all space groups. For example, the body-centered lattice complex, which is given the symbol "I", has symmetry equivalent points at 0,0,0 and 1/2,1/2,1/2 within the unit cell. This occurs in 38 space groups with orthorhombic or higher symmetry.

The "characteristic space-group type" of a lattice complex is defined as the highest symmetry space group that can generate the lattice complex. All other space groups with the same lattice complex are subgroups of that characteristic space group, but not all the subgroups contain the lattice complex (i.e., being a subgroup is a necessary but not sufficient condition). For lattice complex I, the characteristic space-group type is $Im\bar{3}m$; and the "characteristic space-group site" is $m\bar{3}m$ at Wyckoff position a in space group $Im\bar{3}m$, which is a fixed point with zero degrees of freedom.

5.2 Invariant Lattice Complexes and Limiting Complexes

Any lattice complex that has its characteristic space-group site on a fixed point is called an invariant lattice complex. Those with one degree of freedom are called univariant lattice complexes, etc. There are 25 invariant lattice complexes. Listed in order of the number of points [n] per cell in a lattice complex, they are: [1] P; [2] C, E, G, I; [3] J, N, +Q, R; [4] vD, F, +Y; [6] J*, W; [8] D, vT, +Y*; [9] M; [12] S, +V, W*; [16] T, Y**; [24] S*, V*. The lattice complex W* for example is called a twelve pointer. Those equivalent to Bravais lattices are P, C, I, R, and F.

Assigning all Wyckoff positions of all space groups to lattice complexes produces a total of 402 lattice complexes, which are tabulated in Fischer, Burzlaff, Hellner, and Donnay[41] and Fischer and Koch.[43] Our main interest is point configurations resulting from limiting lattice complexes rather than the general lattice complexes as such. A lattice complex such as the invariant "I" can be a subset of a univariant (or divariant) lattice complex. For example, the univariant Wyckoff position 16(c) of space group $I\bar{4}3d$ (#220) produces "I" when the variable x in x,x,x (i.e., on the body diagonal 3-fold axis) is set to zero, but it also has a Y** site at x = 1/8.

These subset special positions are not identified in the lattice complex tables,[43] and it necessary to consult tabulations such as Koch[42] to find them. Unfortunately, only the cubic space groups have been analyzed in this manner. See Koch and Fischer[45] for additional details about this subject called the limiting complexes of lattice complexes. The tabulation of cubic point configurations by Koch[42] lists the locations of all point positions with fewer than three degrees of freedom related to sphere packing and Dirichlet partitions within the cubic space group family as well. We use the Koch tabulation to identify those lattice complexes of the critical net that are invariant.

5.3 Lattice Complex Splitting Equations

The lattice complexes used in Figs. 5.1, 5.2, 5.3, and 5.4 are P, I, F, T, D, J*, W*, E, and N denoting primitive, body-centered, face-centered, tetrahedral, diamond, jack-shaped (from the "pick up jacks" children's game), non-intersecting (German: windschief), hexagonal (Italian: esagonale), and net, respectively. Symbols with a 2 subscript (e.g., P_2) indicate doubling in all three directions to give 8 times as many points. Similarly, P_c indicates a doubling along the c-axis of the unit cell. A superscript number denotes the degree of positional freedom at that site.

The lattice-complex splitting equations[40,41] for the cubic lattice complexes interrelate the lattice complexes. These include I=P+P", P_2=F+F", P_2=I+J*, J*=J+J^, W*=W+W^, F=P+J, D=F+F', D"=F"+F"', and I_2=D+D" with ', ", and "' denoting translations along a body diagonal by (1/4,1/4,1/4), (1/2,1/2,1/2), and (3/4,3/4,3/4), re-

spectively, and ^ denoting translation along a cell edge such as (1/2,0,0). In our analysis of critical nets, these equations relate a lattice complex in one net to a path between two lattice complexes in a net at a lower level. In Fig. 5.1, for example, the P_2 lattice complex in $Im\bar{3}m$ is related to the two F lattice complexes in $Pn\bar{3}m$ and the 3-fold path between them by P_2=F+F". In general, equations with " correspond to paths along 3-fold axes and those with ^ to paths along even-order axes.

5.4 BCC Symmetry Breaking Family

In order to point out some additional properties about orbifolds and critical nets on orbifolds, we examine a series of related cubic space group orbifolds that accommodate the body-centered cubic critical net. The series of cubic space group orbifolds that are related by group/subgroup relationships starting with $Im\bar{3}m$ is shown in the linearized critical nets of Fig. 5.1, which includes the cesium chloride and body-centered cubic critical net crystal structure types.

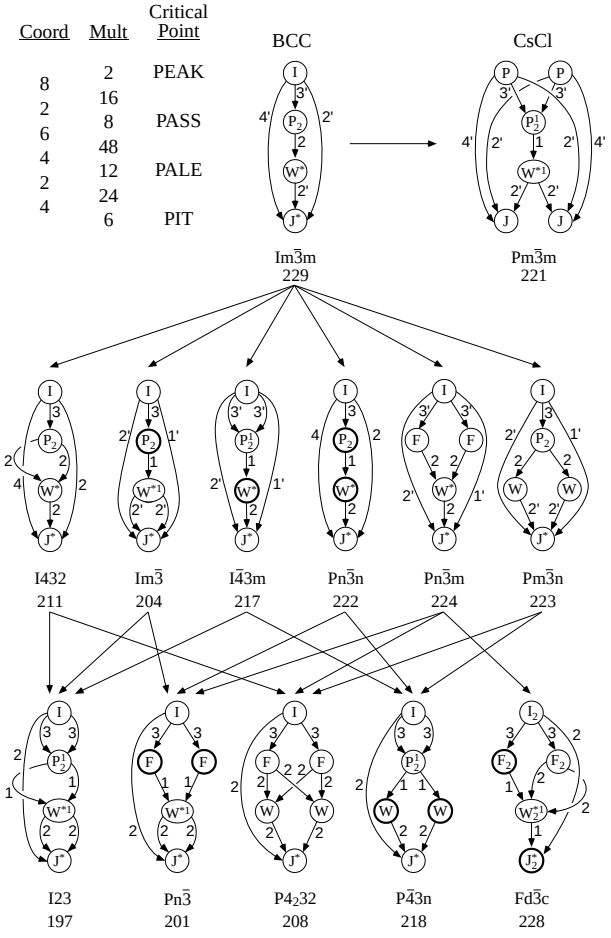

Figure 5.1. Body-centered cubic and CsCl critical nets superimposed onto cubic space group orbifolds.

Notes on orbifold Figs. 5.1, 5.2, and 5.3:

- A straight arrow between graphs points toward a normal subgroup, a straight arrow within a graph points toward a site of "lower density", an arrow between adjacent levels within a graph indicates a critical net Morse function separatrix, and an arrow between nonadjacent levels within a graph indicates a symmetry axis of the space group orbifold that is not embedded into the critical net Morse function.
- A number greater than 1 labeling a line of a graph indicates a 2-, 3-, 4-, or 6-fold crystallographic rotation axis while 1 indicates a path within a general position zone.
- A primed number indicates the path lies in a mirror.
- A thick circle indicates a projective plane suspension point arising from an inversion point not in a mirror (i.e., types b and e of Fig. 2.3).
- For a group/subgroup pair, each axis within the parent graph is either split into two identical axes or reduced in group order by one half (e.g., 4' $\rightarrow$ 4' + 4', 4' $\rightarrow$ 4, or 4' $\rightarrow$ 2') in the subgroup graph.
- A superscript number on a lattice complex symbol denotes the degree of positional freedom at that site.
- Mult, the sum of Wyckoff multiplicities for a row of elements in a graph, is the same for all groups in the illustration except Fd3c (#228), which has 8 times that number because of its multiple cell (e.g., I $\rightarrow$ I_2) lattice complexes.
- Integer ratios of adjacent multiplicities provide the coordination vector.
- The odd-order 3-fold axis in an orbifold is the only operator that can:
  - Continue through a 332 or 3'3'2' junction
  - Bridge a mirror over itself without breaking the mirror if it is 3'3'
  - Permit a 2-fold axis to continue through a 322 or 3'2'2' junction

  In other words, separate edges of a graph can represent different segments of the same Wyckoff site if a 3-fold axis is present.

Notes specific to Fig. 5.1:

- By adding the shortest peak-to-pit path (4' for #229) to the graph, we also obtain the number of peaks around pits (2) and pits around peaks (6) as coordination numbers. The extended coordination vector [e.g., (6)(8,2,6,4,2,4)(2) for bcc] can be used as a local topological description of critical net coordination topology for simple critical nets.
- The underlying topological spaces for Fig. 5.1 are the 3-ball in #229, #221, #224, and #223; S^3 in #211 and #208; RP^3 in #197; doubly suspended RP^2 in #222, #201, #218, and #228; and 3-ball plus singly suspended RP^2 in #204 and #217.

5.5 Additional Cubic Space Group Examples

The face-centered cubic and the diamond families are shown in Figs. 5.2 and 5.3, respectively.

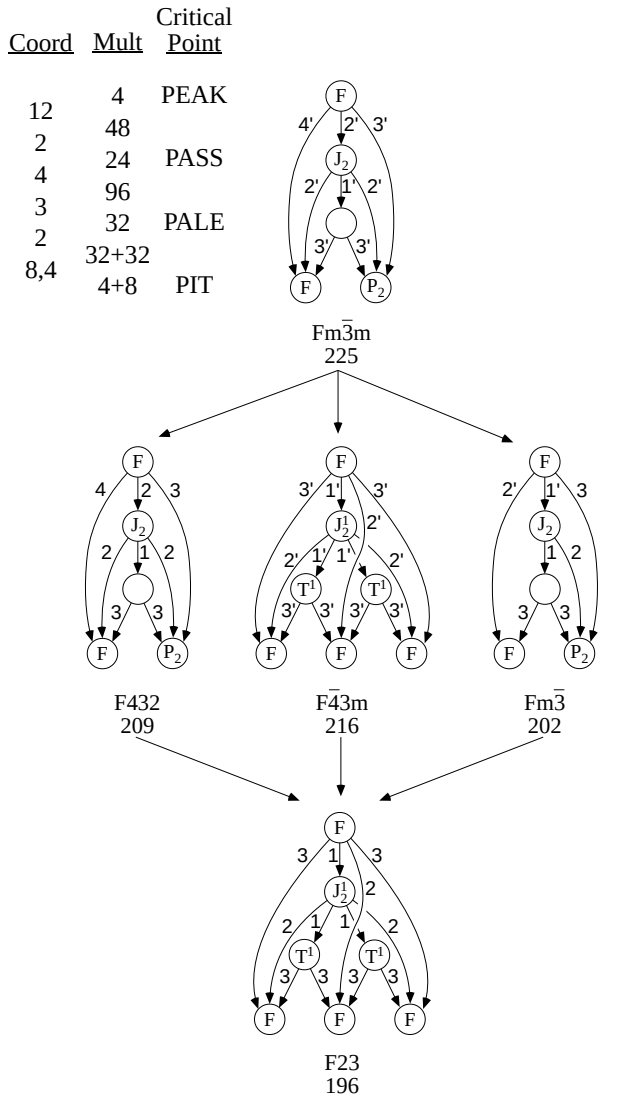

Figure 5.2. Face-centered cubic critical net superimposed onto cubic space group orbifolds.

See "Notes on orbifold Figs. 5.1, 5.2, and 5.3" following Fig. 5.1.

Notes specific to Fig. 5.2:

- Graph nodes that are blank (i.e., without a lattice complex descriptor) are still lattice complexes but do not have a parent on an invariant fixed position and thus do not have a standard crystallographic name.
- The 3' axis in orbifold #216 and the 3-fold axis in #196 extend through all four F lattice complexes, 3'3'2' and 332, respectively, to form loops.
- A single mirror covers orbifold #216.
- The underlying topological spaces are the 3-ball in #225, #216 and #202 and the 3-sphere in #209 and #196.

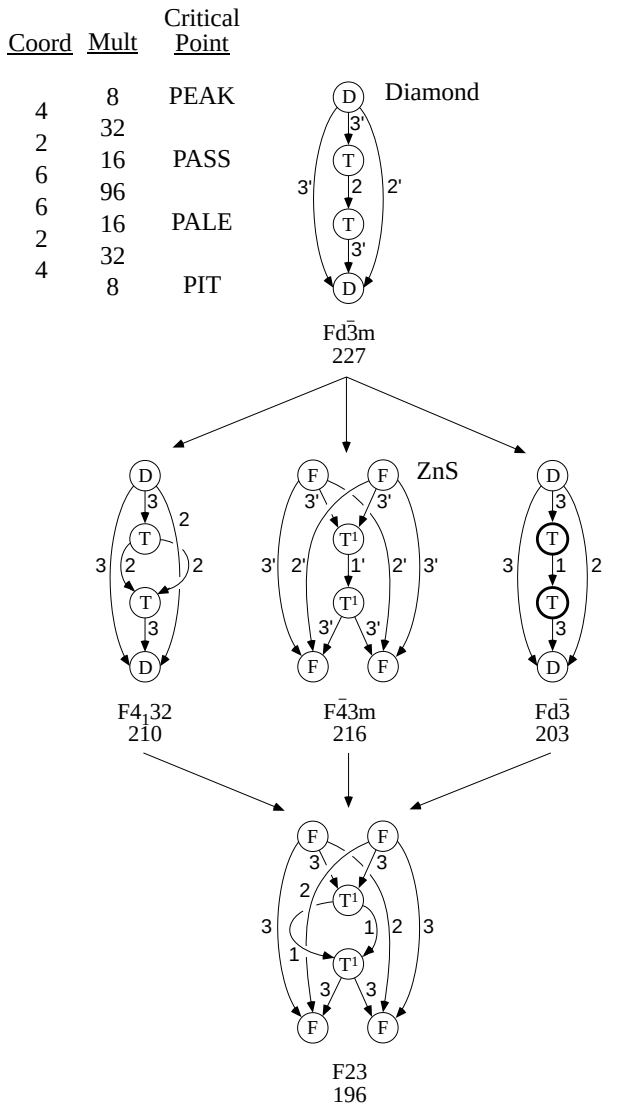

Figure 5.3. Diamond and ZnS critical nets superimposed onto cubic space group orbifolds.

Note specific to Fig 5.3:

- The underlying topological spaces are the 3-ball in #227 and #216, the 3-sphere in #210 and #196, and the doubly suspended projective plane in #203.

5.6 Hexagonal Space Group Examples

Fig. 5.4 shows the critical nets for graphite, hexagonal diamond, and hcp, which all crystallize in the same hexagonal space group, $P6_3/mmc$. The Wyckoff set and orbifold for that space group also are shown.

The nodes of the critical net graphs in Fig. 5.4 contain the appropriate Wyckoff symbol rather than the lattice complex symbols. The Wyckoff to lattice complex mapping is a,b $\rightarrow$ Pc; c,d $\rightarrow$ E; and g $\rightarrow$ N, where Pc stands for primitive with doubling along the c axis.

The upper left drawing of Fig. 5.4 is the orbifold that has a single 2' axis, h, extending around the upper edge of the kitchen measuring-scoop shaped basin. There are three 3' axis intersections (b, c, & d) that h traverses to form a complete loop. The leading end of the scoop has a single 3' axis half-loop, f, while the support spine along the back of the scoop is a second 3' axis, e. The bottom point, a, at the spine, e, gives rise to a 2 axis that goes through open space from point a to point g in the forward end of the scoop. Everything below the 2' axis, h, is covered by mirror floor, k, while that above h has a mirror ceiling, j.

The hcp critical net in the upper right has the multiplicities shown for each critical net component and the coordination vector (8)(12;2;4;3;2;8,4)(6,1), which is identical to that for fcc in Fig. 5.2. The summed hcp multiplicities are all smaller than those for fcc by a factor of two because of the supercell in fcc caused by repeating after three layers in fcc versus two layers in hcp.

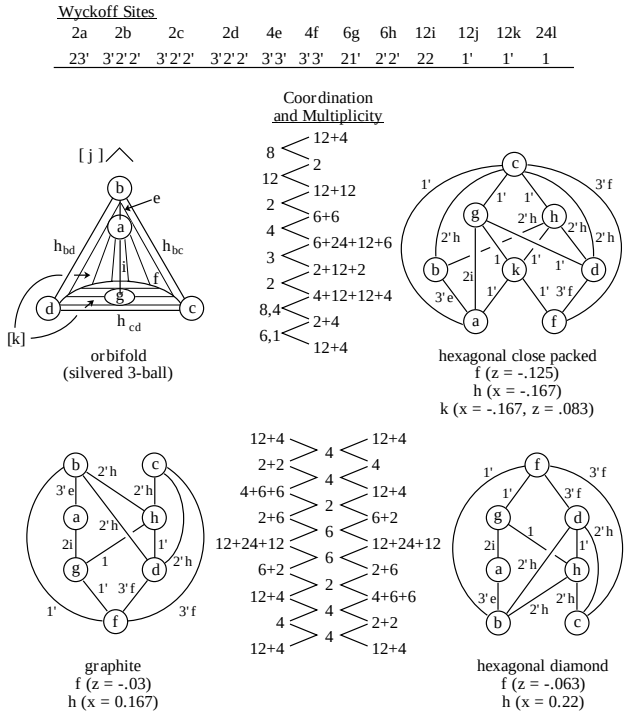

Figure 5.4. Three different critical nets on the hexagonal space group $P6_3/mmc$ orbifold.

An interesting feature of critical nets is duality in which the critical point set's peaks, passes, pales, and pits can be relabeled in inverse order to produce a dual critical net. We note that the diamond structure critical nets shown in Fig. 5.3 are self dual in that there is mirror symmetry relating the top and bottom halves of the critical nets. The face-centered cubic critical nets in Fig. 5.2 and the body-centered cubic critical nets in Fig. 5.1 are not self dual; consequently we can turn those critical nets upside down to produce different families of critical nets.

The bottom two critical-net drawings in Fig. 5.4 illustrate the duality of graphite and hexagonal diamond. Note that the coordination vector (4)(4,2,6,6,2,4)(4) is identical to that for diamond in Fig. 5.3 while the summed multiplicity vector (16)(4,16,8,48,8,16,4)(16) is half that of diamond, which tells us there are more layers in real diamond but the averaged local topology is identical.

The x and z values given under the critical net in Fig. 5.4 provide the variable position parameters for occupied univariate and divariate Wyckoff sites. We felt it necessary to make some slight adjustment in going from graphite to hexagonal diamond based on empirical inspection of stereoscopic ORTEP diagrams. We have not done any analytical positioning of critical points based on the Gaussian density Morse function calculations since for most simple examples studied to date except basic beryllium acetate, the space groups usually provide enough fixed points to define the critical net details. That will not be the case for more complex crystal structure problems where many of the critical points are on general rather than special positions.

5.7 Critical Nets Versus Dirichlet Partitioning

Dirichlet partitioning of 3-space around a lattice-complex point is carried out by placing planes normal to vectors between neighboring points of the complex at midpoints of the vectors. This forms a convex polyhedron around the origin site in which all points within the polyhedron are closer to the origin site than to any other site of the complex. The vertices of a Dirichlet polyhedron are sometimes called interstices, implying holes between spherical atoms.

For the invariant lattice complex P, which represents simple cubic packing, the center, face, edge, and vertex barycenters (centroids) fall on the peak, pass, pale, and pit critical points of the critical net, respectively, as expected. For the body-centered lattice complex I, this correlation does not hold since the bcc peaks, passes, pales, and pits are on the center, 8 hexagonal faces, 24 vertices, and 6 square faces, respectively, rather than on the center, 14 faces, 36 edges, and 24 vertices of the bcc truncated octahedron Dirichlet polyhedron.

Because of such discrepancies, we recommend that critical nets be used in place of Dirichlet polyhedra tiling when practical. The Dirichlet partitioning algorithm is not based on Morse theory topology principles. Thus the bcc rhombohedral dodecahedron coordination polyhedron (12

faces, 24 edges, 14 vertices) is not dual to the bcc truncated octahedron Dirichlet polyhedron,[46] and it serves as a classic counterexample to the postulated duality between corresponding coordination and Dirichlet polyhedra, which the unwary may assume to be present.

6. Where do we go from here?

Since there is little crystallographic background literature available to provide guidance for future research, we present our list of research needs in crystallographic topology. The current state of the art can only be characterized as exploratory. As Walt Kelly's comic strip character Pogo once said, "We are faced with insurmountable opportunities."

6.1 Interpretation of Macromolecule Electron Density Maps

We first got into crystallographic topology in 1976 using critical point analysis as a representation method for heuristic reasoning interpretation of protein electron density maps.[39] The ORCRIT computer program we wrote at that time was "decommissioned" for 15 years but has recently been reactivated and used successfully in a series of feasibility study by Janice Glasgow, Suzanne Fortier, and their Queens' University colleagues.[47] The ORCRIT program is more oriented toward numerical analysis (i.e., 3-D linear blending interpolation and Newton iteration) and graph theory (i.e., minimal spanning trees) than topology. It uses only the peak and pass critical points to construct what might be called ridge lines which tend to trace the polymeric backbone and sidechains.

If we rewrite ORCRIT today, we would use Eric Grosse's spectral spline method[48] to find the critical point set, then numerically trace the separatrices. From the resulting critical net we can determine volume, integrated density, and topological shape descriptors for the chemical cages for computational comparison with related archived peptide and protein structure results. ORCRIT relied entirely on distance, angle, and critical-point eigenvector metric details, which are intrinsically less robust than integrated quantities and topological descriptors.

6.2 Critical Net Software Needs

We need to develop computer programs to determine routine critical nets for small molecule crystal structures such as basic beryllium acetate, shown in Fig. 3.5. We present a "wish list" of what we would like to develop or see developed by others. We need to:

- Write a modified ORCRIT program that, through summation of crystal space Gaussian density functions, can calculate density and its first two derivatives at any point in an asymmetric unit. ORCRIT can then do its pattern search for critical points without storing or interpolating density maps on grids.
- Write a "twisted H" search function for ORTEP based on the comments in Sect. 3.9 to assign critical net indices and separatrices.
- Modify ORTEP-III to more automatically plot critical net drawing given the critical points and separatrices. The current features are minimal.
- Write a matroid[49] program to resolve hierarchically the orbifold singular set in one direction and the crystal structure critical net in a second direction. Such a program could provide a representation for crystal structure classification, archiving, and querying. This "dimatroid" could also serve as a "blackboard representation" in heuristic programming for stepwise conversions of $Fd\bar{3}$ (in Fig. 5.3) to the full basic beryllium acetate critical graph, for example.

6.3 Orbifold Atlas

The orbifold atlas we have mentioned several times is needed for both pedagogical and research reference purposes. For each space group the atlas might include two identical orbifold singular sets drawings with Wyckoff site symbols on one and lattice complex plus axis order numbers symbols on the other. Perhaps the simplest possible linearized critical net graph(s) for that space group might also be presented. There should also be a list of coordinates for the fundamental domain (asymmetric unit) vertices used based on the ITCr[1] space group drawing selected. A brief description of the underlying topological space and the key orbifolding steps used to close the fundamental domain should also be included.

In addition to a sequential ordering of orbifolds based on the standard space group numbers, subgroup/lattice-complex trees of linearized critical net graphs such as Figs. 5.1, 5.2, and 5.3 could be made for the various crystal families. A nomenclature system based on such graphs would be useful in crystal structure classification.

Graphics automation of singular set drawing would certainly be welcome and perhaps essential since the existing computer-assisted drawing programs such as Adobe Illustrator are very labor intensive when applied to this task. One approach is to use a graphics techniques of knot theory where Möbius energy functions based on Coulomb's law are applied to space curves, links, knotted graphs, surfaces, and other submanifolds.[50] Programs such as Scharein's KnotPlot, Brakke's Surface Evolver and the Geometry Center's GeomView, which are all described on the World Wide Web, might be adapted to this task.

6.4 Interactive Data Base for Space Groups and Orbifolds

Existing commercial space group data base programs have not been useful in our research. We would like to see a noncommercial World Wide Web site that provides the key information of the ITCr[1] for any space group including Wyckoff sites and subgroup family data. An interac-

tive orbifold atlas could be implemented through addition of database retrieval for topological orbifold data.

The computer algebra system GAP,[51] which stands for Groups, Algebra and Programming, was developed by Joachim Neubueser and coworkers of Lehrstuhl D für Mathematik, RWTH, Aachen, Germany. GAP now contains a crystallographic library for two, three, and four dimensional space groups based on the tables of Brown *et al*.[52] A WWW server might be feasible that would combine orbifold data bases and the GAP system to provide interactive answers to both standard and research level inquiries about crystallographic groups and orbifolds.

6.5 Orbifold Covers Based on Color Groups

The bicolor Shubnikov space groups and other crystallographic color groups[26] have both symmetry and antisymmetry group elements with the symmetry elements carrying out the normal positional transformation operations. The antisymmetry elements of an n-color group are essentially the elements of a group that are deleted in going from a group to one of its index-n normal subgroups. The color groups are often used in crystal physics applications such as the description of magnetic patterns in crystal structures, but they can be used here to describe the cover of an orbifold or to derive one Euclidean 3-orbifold from another 3-orbifold when their parent space groups have a group/n-index normal subgroup relationship.

We have derived graphical representations for the 58 bicolor spherical 2-orbifolds to supplement Fig. 2.3 and it would not be difficult to extend this to the bicolor plane groups. Full bicolor illustrations of the 1191 nontrivial Shubnikov space groups are given in Koptsik[53] but the complexity of those illustrations is quite overwhelming. An atlas of Euclidean bicolor 3-orbifold drawings is perhaps feasible but not a trivial project.

Using GAP, it should be possible to rederive the Shubnikov space groups computationally and from them derive the ordinary Euclidean 3-orbifolds in space group/subgroup families starting from a small number of top level orbifolds in each family derived with normal geometric topology cut-and-paste methods.

6.6 Analytical Topology

Although there is a huge analytical topology literature that should seemingly be applicable to crystallographic topology problems, the only equation that we have found really useful in practice is the Euler-Poincare equation, which states that the alternating sum for the numbers of the sequential critical point types is zero for Euclidean manifolds of all dimensions. We need equivariant invariants for characterization of orbifolds, underlying topological spaces of orbifolds, and crystallographic Morse functions on space groups and orbifolds. We anticipate that such invariants probably involve cohomology.[7,31,32,33]

Thurston[16,17,54] conjectures that each closed 3-manifold can be decomposed (by connected sums and splitting along incompressible tori) into pieces, each of which has a geometric structure modeled on one of eight types of 3-dimensional geometries—H^3, Sol, S^3, E^3, $S^2\times R$, $H^2\times R$, Nil, and (the universal cover of) SL(2,R). Structures on Seifert manifolds account for the last six of the eight geometries. Several of the underlying spaces for orientable 3-orbifolds have S^3 (for dihedral point groups) and $S^2\times R$ (for cyclic point groups) as underlying spaces, and the 10 Euclidean manifolds have Seifert manifolds as underlying spaces. Are there any formal theorems that give all the underlying spaces for Euclidean 3-orbifolds in terms of specific classes of geometries or manifolds?

At times we need to trace geodesic paths in orbifolds corresponding to general straight lines in Euclidean crystal space. For Euclidean and spherical 2-orbifolds, conformal mapping, using the Schwarz-Christoffel transformation from an arbitrary circle or half plane (orbifold) to an n-gon (fundamental domain), and analytic continuation, based on Schwartz's principle of reflection, will work assuming the reverse transformation also is available. However, our problems are mainly 3- rather than 2-dimensional. The literature on Riemannian orbifolds (e.g., Riemannian geometry of orbifolds[55]) should be followed for its relevance to this problem.

Appendix

The 36 cubic crystallographic space groups are different from the remaining 194 space groups in that they each have body diagonal 3-fold axes arising from their tetrahedral and octahedral point groups. These body diagonal 3-fold axes make their orbifolds a less understood topology problem in that the Siefert fibered spaces approach of lifting from a base Euclidean 2-orbifold is inapplicable since fibration along the required orthogonal projections become tangled together by the 3-fold axes. On the other hand, many aspects of the cubic groups orbifolds are more straightforward than for the simpler space groups that are based on cyclic and dihedral point groups.

The 36 Euclidean 3-orbifolds for the cubic space groups (i.e., the cubic 3-orbifolds) are illustrated in Figs. 2.8 of Sect. 2 and A.1 of this Appendix. The 12 cubic 3-orbifolds in Fig. 2.8 have S^3 as their underlying topological space. For the 24 cubic orbifolds in Fig. A.1, the first 11 have a 3-ball underlying space, the next two have singly suspended projective 2-planes (RP^2) with mirror boundary, followed by 10 with doubly suspended projective 2-planes (RP^2). The final cubic 3-orbifold in Fig. A.1 has a projective 3-plane (RP^3) underlying space.

The small circles at the points of each projective plane cone in Fig. A.1 denote projective plane suspension points which arise from mirror-free inversion centers of the space groups. The dashed lines around the circumference denote the antipodal relationship for points halfway around each circle on the cone surface. The dashed line around the RP^3 sphere denotes an antipodal gluing

relationship for all points on any great circle of the RP^3 spherical representation. Orbifolds having an RP^2 or RP^3 underlying space may be drawn in several different ways because of the sliding antipodal gluing relationship for projective planes discussed in Sect. 2. For the RP^2 examples in Fig. A.1, drawings with the least possible number of singular-set components on the antipodal surface are shown. However, to visualize critical-net-on-orbifold drawings such as those in Fig. 5.1, it is often necessary to move certain axes onto the antipodal gluing surface since this is one of the mechanisms for the singular set splitting discussed in Sect. 5.

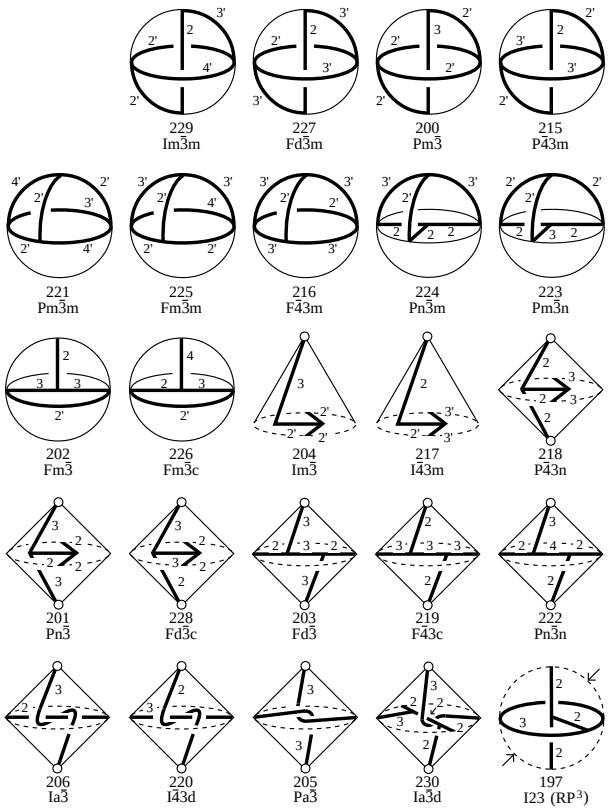

Figure A.1. The 24 cubic 3-orbifolds that do not have S^3 as the underlying topological space.

Each cubic group has an index-4 rhombohedral based trigonal subgroup and an index-3 orthorhombic or tetragonal subgroup. There are only seven rhombohedral space groups: R3 (3), R32 (32), R$\bar{3}$m and R$\bar{3}$c ($\bar{3}$m), R3m and R3c (3m), and R$\bar{3}$ ($\bar{3}$) where the symbol in parentheses is the corresponding trigonal point group. Thus it seemed a reasonable approach to order the cubic groups in columns according to their index-4 rhombohedral subgroups and in rows according to their index-2 cubic subgroups. After some additional partitioning of R$\bar{3}$m and R$\bar{3}$c columns we arrived at the subgroup graph shown in Fig A.2. We thank John H. Conway of Princeton for an e-mail exchange explaining his related "odd-subroutine" approach to the group classification problem that he has applied to a number of group classification problems including the crystallographic space groups.

Fig. A.2 uses the subgroup, group normalizer, and lattice complex information given in the ITCr.[1] Each box contains the cubic space group symbol in the upper right subbox, the index-3 orthorhombic or tetrahedral subgroup in the middle, and their respective ITCr sequence numbers on the bottom line. The upper left subbox contains the simplest lattice complex of the cubic space group. Orbifolds for the index-3 subgroups of the cubic groups can be used to derive the cubic orbifolds. Boldface type identifies group normalizers, and group normalizer basins are identified by bold solid lines leading down from cubic (but not orthorhombic) group normalizers.

The seven rhombohedral trigonal subgroups of the cubic groups are shown in the bottom row of the figure with their space group symbols and simplest lattice complex in the top row of each box. The index-3 subgroups (monoclinic/triclinic) of the rhombohedral groups are indicated on the middle line and the respective ITCr numbers on the bottom line of each box. The divider strip between the cubic and rhombohedral groups gives the point groups for all the space groups involved in each column, with the cubic/orthorhombic (or tetragonal) to the left and the rhombohedral/monoclinic (or triclinic) to the right.

Two boxes in a row that are not separated by a space belong to a specific column. To minimize clutter in the drawing we use the convention that whenever a subgroup connection line goes to the midline separating adjacent boxes, both boxes are involved in the subgroup relation. If that line goes to another pair of adjoined boxes, the right goes to the right and the left to the left except when there is a loop in the subgroup relation line, which indicates a right-left interchange. All solid lines join order-2 subgroups and pertain to the cubic, orthorhombic/tetragonal, rhombohedral, and monoclinic/triclinic sets of groups individually. The orthorhombic space group set forms pairs of duplicates.

The dashed lines leading to a dashed box two levels further down is an index-4 subgroup relationship. Note that each dashed box is a repeat of the regular box three levels up in the same column, reflecting the Bravais lattice repetition I, P, F, I, P which occurs in each column as denoted by the initial letters in the space group symbols. This relationship only holds for the cubic space groups in the figure and not for the orthorhombics/tetragonals. Since Fig. A.2 is meant to be used mainly for orbifold applications, it does not include explicit information on how many unit cells are required for each space group/subgroup relationship.

Note that for order-2 subgroups, there are two independent cubic space group families, one starting at Im$\bar{3}$m and ending at F23, and the second starting at Ia$\bar{3}$d and ending at $P2_13$. The ending space groups are the only two cases of space groups without order-2 subgroups. The two series are sometimes called the A and B cubic space group families, respectively.

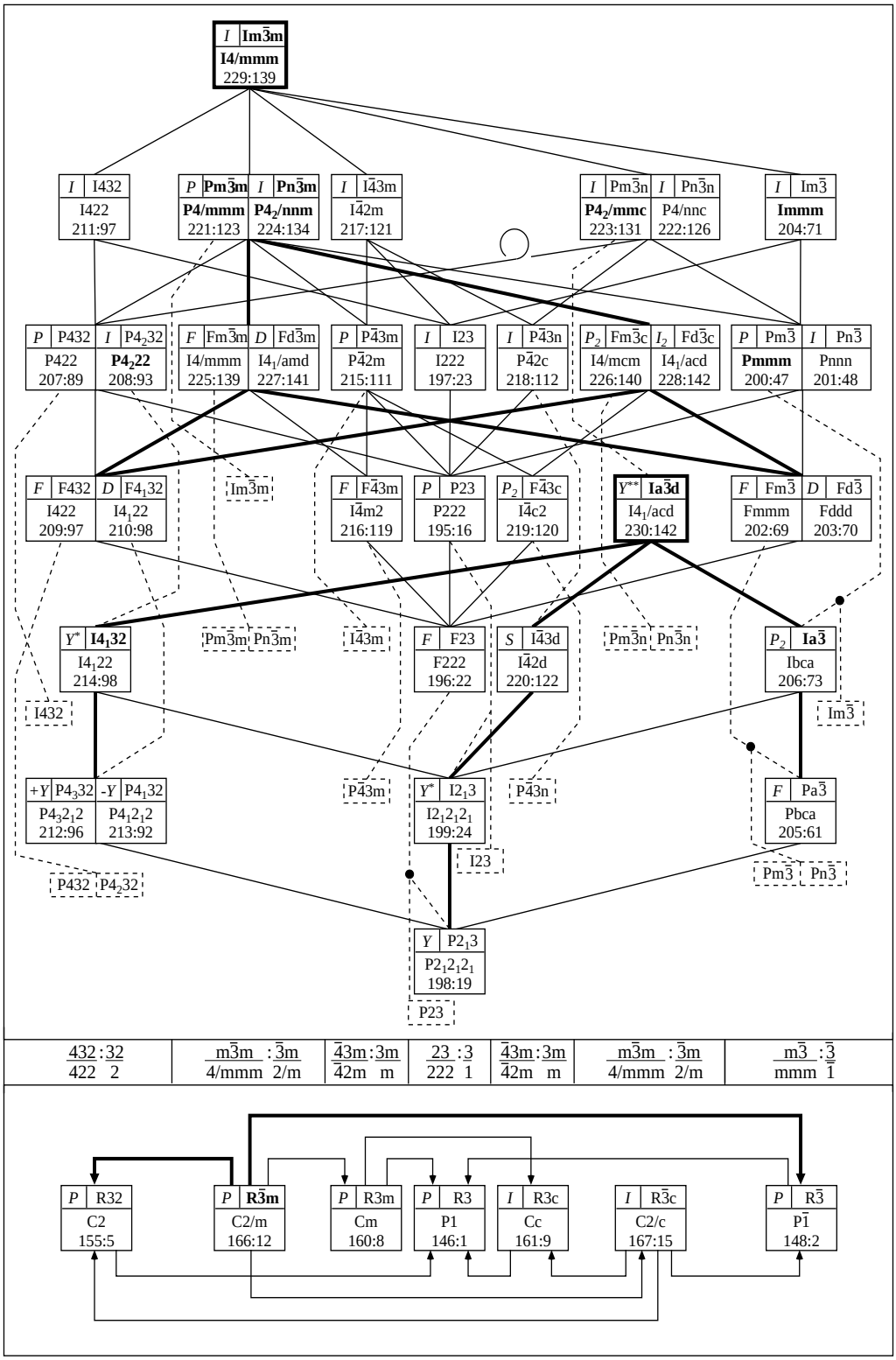

Figure A.2. Cubic space group/subgroup graph.

Solid lines = index 2; dashed lines and rhombohedral column subgroups = index 4; space groups in lower parts of boxes = index 3.

References

[1] T. Hahn, ed., *International Tables for Crystallography, Volume A: Space-Group Symmetry*, Kluwer Academic Publishers, Dordrecht, The Netherlands, 1995.

[2] M. Morse and S. S. Cairns, *Critical Point Theory in Global Analysis and Differential Topology: An Introduction*, Academic Press, 1969.

[3] J. Milnor, *Morse Theory*, Princeton University Press, Princeton, New Jersey, 1969.

[4] M. Goresky and R. MacPherson, "Stratified Morse Theory" in *Proc. Symp. Pure Math.*, Vol. 40, pp. 517-533, 1983; M. Goresky and R. MacPherson, Stratified Morse Theory, Springer-Verlag, New York, 1988.

[5] L. E. El'sgol'c, *Qualitative Methods in Mathematical Analysis*, American Mathematical Society, Providence, Rhode Island, 1964.

[6] M. N. Burnett and C. K. Johnson, *ORTEP-III: Oak Ridge Thermal Ellipsoid Plot Program for Crystal Structure Illustrations*, ORNL-6895, Oak Ridge National Laboratory, 1996.

[7] A. Dimca, *Singularities and Topology of Hypersurfaces*, Springer-Verlag, New York, 1992.

[8] C. T. C. Wall, "Deformations of Real Singularities," *Topology*, Vol. 29, pp. 441-460, 1990.

[9] R. F. W. Bader, *Atoms in Molecules—A Quantum Theory*, University Press, Oxford, 1991.

[10] S. Barr, *Experiments in Topology*, Dover Publications, Inc., New York, 1964.

[11] G. McCarty, *Topology: An Introduction with Application to Topological Groups*, Dover Publications, Inc., New York, 1967.

[12] D. Rolfsen, *Knots and Links*, Publish or Perish, Inc., Houston, Texas, 1990.

[13] L. C. Kinsey, *Topology of Surfaces*, Springer-Verlag, New York, 1993.

[14] K. Ito, ed., *Encyclopedic Dictionary of Mathematics*, Second Ed., The MIT Press, Cambridge, Massachusetts, 1987.

[15] I. Satake, "On a Generalization of the Notion of a Manifold," *Proc. Nat. Acad. of Science USA*, Vol. 42, pp. 359-363, 1956.

[16] W. P. Thurston, "Three-Dimensional Geometry and Topology," The Geometry Center, University of Minnesota, 1992.

[17] P. Scott, "The Geometry of 3-Manifolds," *Bull. Lond. Math. Soc.*, Vol. 15, pp. 401-487, 1983.

[18] W. D. Dunbar, "Fibered Orbifolds and Crystallographic Groups," Ph.D. Dissertation, Princeton University, 1981.

[19] W. D. Dunbar, "Geometric Orbifolds," *Rev. Mat. Univ. Comp. Madrid*, Vol. 1, pp. 67-99, 1988.

[20] F. Bonahon and L. Siebenmann, "Seifert 3-Orbifolds and Their Role as Natural Crystalline Parts of Arbitrary Compact Irreducible 3-Orbifolds," unpublished, 1983.

[21] F. Bonahon and L. Siebenmann, "The Classification of Seifert Fibered 3-Orbifolds" in *Low Dimensional Topology*, Cambridge University Press, pp. 19-85, 1985.

[22] J. M. Montesinos, *Classical Tessellations and Three-Manifolds*, Springer-Verlag, New York, 1987.

[23] J. H. Conway, "The Orbifold Notation for Surface Groups" in *Groups, Combinatorics & Geometry*, M. Liebeck and J. Saxl, eds., Cambridge University Press, pp. 438-447, 1992.

[24] J. Conway and B. Thurston, "Two and Three-Dimensional Euclidean Orbifold Voodoo," preprint.

[25] W. S. Massey, *Algebraic Topology: An Introduction*, Springer-Verlag, New York, pp. 145-180, 1967.

[26] R. L. E. Schwartzenberger, "Colour Symmetry," *Bull. London Math. Soc.*, Vol. 16, pp. 209-240, 1984.

[27] P. Orlik, *Seifert Manifolds*, Springer-Verlag, New York, 1972.

[28] J. A. Wolf, *Spaces of Constant Curvature*, 5th Ed., Publish or Perish, Inc., Wilmington, Delaware, 1984.

[29] C. K. Johnson and H. A. Levy, "Thermal-Motion Analysis Using Bragg Diffraction Data," *International Tables for X-Ray Crystallography, Volume IV*, J. A. Ibers and W. C. Hamilton, eds., The Kynoch Press, Birmingham, England, pp. 311-334, 1974.

[30] L. van Hove, "The Occurrence of Singularities in the Elastic Frequency Distribution of a Crystal," *Phys. Rev.*, Vol. 89, pp. 1189-1193, 1953.

[31] E. Bierstone, *The Structure of Orbit Spaces and the Singularities of Equivariant Mappings*, Instituto de Matematica Pura e Aplicada, Rio de Janeiro, 1980.

[32] E. Lerman and S. Tolman, "Hamiltonian Torus Actions on Symplectic Orbifolds and Toric Varieties," Differential Geometry Preprint #dg-ga/9511008, 1995.

[33] F. C. Kirwan, *Cohomology of Quotients in Symplectic and Algebraic Geometry*, Princeton University Press, Princeton, New Jersey, 1984.

[34] A. W. M. Dress, D. H. Huson and E. Molnár, "The Classification of Face-Transitive Periodic Three-Dimensional Tilings," *Acta Cryst.*, Vol. A49, pp. 806-817, 1993.

[35] E. Molnár, "Symmetry Breaking of the Cube Tiling and the Spatial Chess Board by D-Symbols," *Algebra and Geometry*, Vol. 35, pp. 205-238, 1994.

[36] O. Delgado Friedrichs and D. H. Huson, "Orbifold Triangulations and Crystallographic Groups," *Period. Math. Hung.*, in press.

[37] F. P. Bundy and J. S. Kasper, "Hexagonal Diamond—A New Form of Carbon," *J. Chem. Phys.*, Vol. 46, pp. 3437-3446, 1967.

[38] A. Tulinsky, C. R. Worthington, and E. Pignataro, "Basic Beryllium Acetate: Parts I-III," *Acta Cryst.*, Vol. 12, pp. 623-637, 1959.

[39] C. K. Johnson and E. Grosse, "Interpolation Polynomials, Minimal Spanning Trees and Ridge-Line Analysis in Density Map Interpretation," *Abstracts of the American Crystallographic Association Meeting, Evanston, Illinois, Aug. 9-12, 1976*; C. K. Johnson, "Peaks, Passes, Pales, and Pits: A Tour through the Critical Points of Interest in a Density Map," *Abstracts of the American Crystallographic Association Meeting, Pacific Grove, California, Feb. 21-25, 1977*.

[40] E. Hellner, "Descriptive Symbols for Crystal-Structure Types and Homeotypes Based on Lattice Complexes," *Acta Cryst.*, Vol. 19, pp. 703-712, 1965.

[41] W. Fisher, H. Burzlaff, E. Hellner, and J. D. J. Donnay, *Space Groups and Lattice Complexes*, National Bureau of Standards Monograph 134, 1973.

[42] E. Koch, "A Geometrical Classification of Cubic Point Configurations," *Z. Krist.*, Vol. 166, pp. 23-52, 1984.

[43] W. Fischer and E. Koch, "Lattice Complexes," pp. 825-854 in *International Tables for Crystallography, Volume*

A, T. Hahn, ed., Kluwer Academic Publishers, Dordrecht, The Netherlands, 1995.

[44] E. Hellner, E. Koch, and A. Reinhardt, *The Homogeneous Frameworks of the Cubic Crystal Structures, Physics Data*, Nr. 16-2, 1981.

[45] E. Koch and W. Fischer, "Lattice Complexes and Limiting Complexes Versus Orbit Types and Non-characteristic Orbits: a Comparative Discussion," *Acta Cryst*., Vol. A41, pp. 421-426, 1985.

[46] A. L. Loeb, "A Systematic Survey of Cubic Crystal Structures," *J. Solid State Chem*., Vol. 1, pp. 237-267, 1970.

[47] L. Leherte, S. Fortier, J. Glasgow, and F. H. Allen, "Molecular Scene Analysis: Application of a Topological Approach to the Automated Interpretation of Protein Electron Density Maps," *Acta Cryst*., Vol. D50, pp. 155-166, 1994.

[48] E. H. Grosse, "Approximation and Optimization of Electron Density Maps," Ph.D. Dissertation, Stanford University, Stanford, California, 1980.

[49] A. Björner, M. Las Vergnas, B. Sturmfels, N. White, and G. M. Ziegler, *Oriented Matroids, Encyclopedia of Mathematics*, Vol. 46, Cambridge University Press, Cambridge, England, 1993; G. M. Ziegler, "Oriented Matroids Today," World Wide Web http://www.math.tu-berlin.de/~ziegler, 1996.

[50] R. B. Kusner and J. M. Sullivan, "Möbius Energies for Knots and Links, Surfaces and Submanifolds," preprint, 1994.

[51] Martin Schönert *et al*., *GAP—Groups, Algorithms, and Programming*, Lehrstuhl D für Mathematik, Rheinisch Westfälische Technische Hochschule, Aachen, Germany, first edition, 1992.

[52] H. Brown *et al*., *Crystallographic Groups of Four-Dimensional Space*, John Wiley & Sons, New York, 1978.

[53] V. A. Koptsik, *Shubnikov Groups*, Izd. MGU, Moscow, pp. 212-227, 1966.

[54] W. P. Thurston, "Three-Dimensional Manifolds, Kleinian Groups, and Hyperbolic Manifolds," *Bull. Amer. Math. Soc*., Vol. 6, pp. 357-382, 1982.

[55] J. E. Borzellino, "Riemannian Geometry of Orbifolds," Ph.D. Dissertation, University of California, Los Angeles, 1992.